CHAPTER 2
THEORIES

2.1 Clay minerals

The word clay is used to describe the smallest-size fraction in classical mineral sediments. The maximum size of clay particles, however, is defined differently in different disciplines. Geologists usually use the Wentworth scale, in which clay-sized material consists of particles smaller than 4 μm in a diameter. Soil engineers usually use an upper size boundary of 2 μm. There is no really sharp natural boundary between clay minerals and non-clay minerals at either 2 or 4 μm, but there is a general tendency for clay minerals to break down easily to grains of about 2 μm diameter when dispersed in water, and 2 μm is commonly used for separating clay minerals from other minerals. Clays are composed primarily of the elements silicon, aluminum, oxygen and hydrogen, and thus can be described as hydrous aluminosilicates, but they also contain minor amounts of many metal ions, especially iron(II) and iron(III).

There are two major types of clay mineral, the oxide and the aluminosilicates. The oxide minerals may be either crystalline such as gibbsite ($Al(OH)_3$), hematite (α-Fe_2O_3) or goethite (α-FeO(OH)), or essentially amorphous, without long range structural order. Such poorly crystalline oxides are often closely associated with aluminosilicate minerals, especially in highly weathered environments. The aluminosilicate clay minerals, of which the kaolin used in the present work is an example, can have very diverse structures and compositions. They can be classified into four major groups: **group silicates** with structures based on either isolated SiO_4 tetrahedral (nesosilicates), or condensed groupings such as Si_2O_7 (sorosilicates) and Si_6O_{18} (ring silicates), **chain silicates**, such as pyroxenes and amphiboles with SiO_4 tetrahedra linked to form single and double $(SiO_3)_n$ chains, respectively, **layer silicates**, in which the crystal structures are based upon a hexagonal network of linked silicon-oxygen tetrahedral, and **framework silicates**, such as feldspars in which the SiO_4 tetrahedra form a 3-dimensional structure. Since kaolin is a layer silicate this group of minerals will be considered in more detail in the following section.

2.2 Classification of layer silicate mineral

A brief summary of the main types of layer silicate (also known as phyllosilicates) is presented in Table 2.1. The various minerals differ in terms of both structural arrangements and chemical composition.

Table 2.1 The major phyllosilicate minerals (layer silicates)
(Source: Mackenzie, 1975; Brindley et al., 1968)

Layer type	Group name	Charge per unit formula	Common minerals
1:1	Kaolinite-serpentine	~ 0	Kaolinite, Halloysite Chrysotite, Lizardite, Antigorite
2:1	Pyrophyllite-talc	~ 0	Pyrophyllite and Talc
	Smectite or Nontronite	0.25-0.6	Montmorillonite, Beidellite,
	Montmorillonite-Saponite		Saponite, Hectorite,Sauconite
	Mica	~ 1	Muscovite, Paragonite Biotile, Phlogopite
	Brittle mica	~ 2	Margarite, Clintonite
	Illite	2	Illite
	Vermiculite	0.6-1.9	Vermiculite
2:1:1 chain	Chlorite	variable	Chlorite
	Palygorskite-Sepiolite	-	Palygorskite, Sepiolite

The basic layer silicate structure is formed by combining tetrahedral silica sheets and octahedral alumina sheets. The octahedral are tied to the tetrahedral by sharing the oxygen atoms at the top of the tetrahedral sheet. A mineral formed by combining one tetrahedral sheet with one octahedral sheet is called a 1:1 or **t–o** mineral, whereas the

combination of two tetrahedral sheets on each side of an octahedral sheet produces a 2:1 or **t-o-t** mineral. Isomorphous substitutions in these structures can generate layer charges of different magnitudes, and these determine the nature of the bonding between neighbouring layers, and the ease with which they can be separated by intercalation of solvent or other molecules (Figures 2.1 and 2.2)

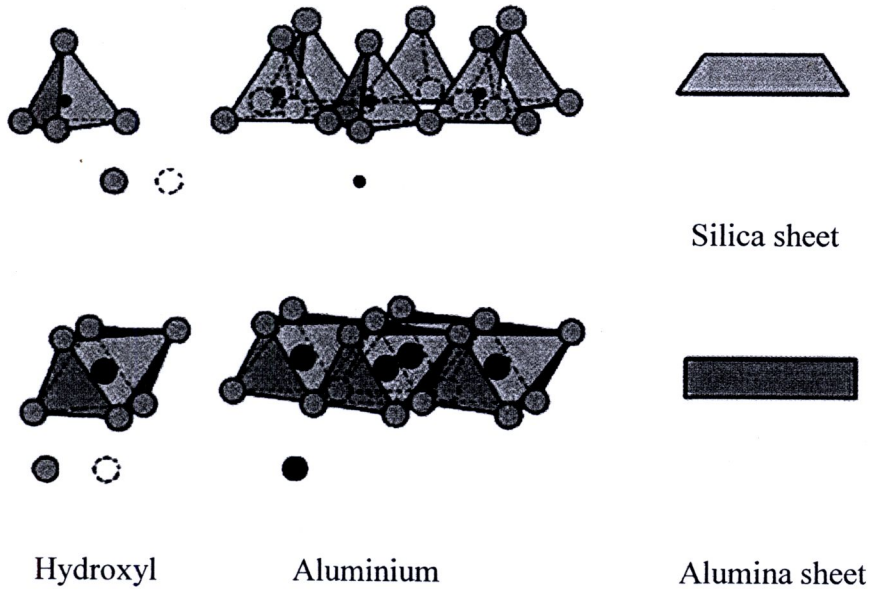

Figure 2.1 Basic units of clay minerals. The silica and alumina sheet (Mitchell, 1993)

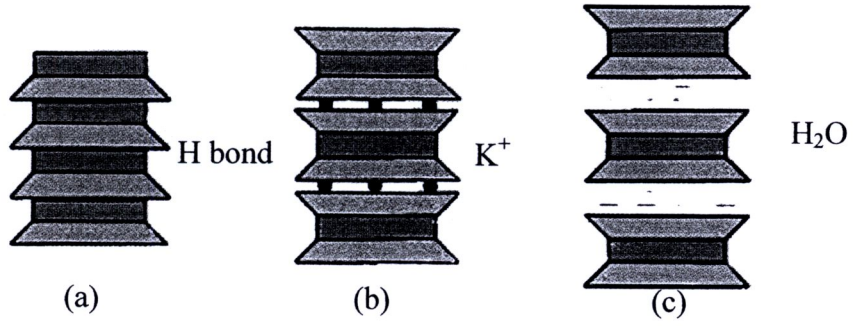

Figure 2.2 Structure of the major clay minerals: (a) kaolinite (b) illite and (c) montmorillonite (based on combined sheets) (Mitchell, 1993)

2.3 Structural characteristics of phyllosilicate minerals

There are fundamental differences in the surface compositions of the 2:1 and 1:1 layer silicates. With the 2:1 minerals, the layer contains an octahedral (alumina) sheet sandwiched between two tetrahedral silica sheets. The two layer surfaces are, therefore,

essentially equivalent and consist of planes of oxygen atoms (siloxane surface), with a distorted hexagonal cavity formed by six-corner sharing silica tetrahedral (Figure 2.3). In nature, some Al can substitute for Si in the tetrahedral sheet, and atoms of lower oxidation states can isomorphously replace some of the Al in the octahedral sheet. Both of these processes produce negatively-charged layers. These negative charges are balanced by intercalation of cations in the interlayer region. In smectites, where there is a relatively small layer charge generated by low levels of isomorphous substitutions in the structure, the low interaction between the layers allows easy separation, the intercalation of solvent molecules, and the easy exchange of interlayer cations. This cation exchange capacity (measured in meq/100g) is a characteristic of the smectite minerals, of which montmorillonite (Figure 2.3) is one of the best known examples.

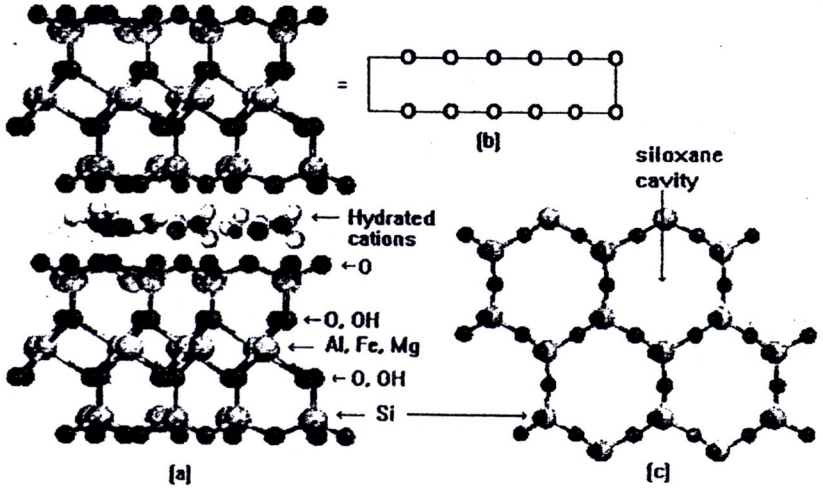

Figure 2.3 (a) Structure of montmorillonite, (b) schematic representation of a single layer, and (c) a top view of the silicate sheet (Wypych and Satyanarayana, 2004)

In kaolinite, the layers are built from a single sheet of silicon tetrahedrally bonded to oxygen atoms and a sheet of aluminum octahedrally bonded to oxygen atoms and hydroxyl groups. As a consequence, the aluminum side of the layer is covered in hydroxyl groups (aluminol), whereas the silicon side contains oxygen atoms (siloxane surface). These characteristics make the kaolinite structure an unique matrix in which any interlayer molecule will be subjected to an asymmetric chemical environment. Adjacent layers of kaolinite are linked to each other by hydrogen bonds involving the aluminol and siloxane groups, and this results in high cohesion between layers which hinders intercalation, grafting and exfoliation reactions. Although there are relatively

small variations in kaolinite composition, this does vary with its genesis, which also affects its degree of crystallinity, and hence its chemical properties. The kaolimite structure is presented in Figure 2.4.

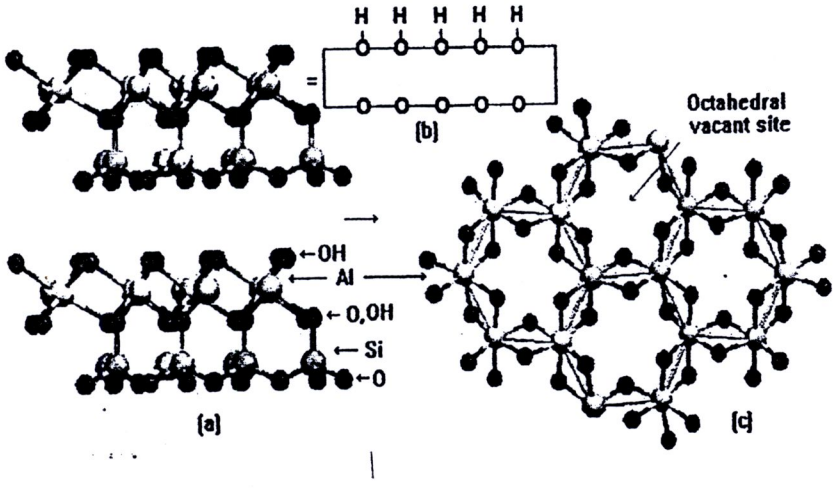

Figure 2.4 (a) Structure of kaolinite, (b) schematic representation of a single layer, and (c) top view of the hydroxide sheet (Wypych and Satyanarayana, 2004)

2.4 Surface chemistry of phyllosilicate minerals

Surface reactions and the corresponding surface complexes play fundamental roles in the behavior and properties of materials with layered structures. Many of the chemical reactions of phyllosilicate minerals are surface phenomena (e.g. cation exchange, adsorption). From the preceding section on clay mineral structures, it follows that clay surfaces can be divided into at least three categories.

1. Surfaces formed mainly by Si-O-Si linkages of silica tetrahedra
2. Surfaces formed by O-Al-OH linkages of alumina octahedra
3. Surfaces formed by -Si-OH or -Al-OH of amorphous compounds

The first category of surface is characterised by oxygen atoms coordinated to the silicon atoms of the tetrahedral sheet. Sticher and Bach (1966) refer to the Si-O-Si bond as a siloxane bond and the siloxane surface is typical of the 2:1 type of phyllosilicate clay. The charge on a siloxane surface can originate from isomorphous substitution of Al for Si atoms in the tetrahedral sheets, or a divalent ion for Al in the octahedral sheet.

The second type of clay surfaces is characterised by planes of exposed OH groups, underlain by Al, Fe, or Mg atoms in the octahedral sheet. Kaolinite and other 1:1 phyllosilicate minerals have a siloxane surface on one basal plane, and a hydroxide surface on other basal plane. The exposed hydroxyl groups are able to dissociate and can, therefore, play an important role in the development of negative charges.

The third type of surface is formed by -Si-OH (silanol), -Al-OH (aluminol), or –Fe-OH (ferrol) groups. Such surfaces are typically present in silica gel, amorphous Al-and Fe-oxides, or allophane.

2.4.1 Surface area

For quantitative interpretation of the properties of clay minerals, information is needed on their surface areas as well as their surface compositions. Rates of adsorption are proportional to surface areas, which can also have a strong influence on cation exchange. The surface area generally increases with decreasing particle size, and can be measured by several methods (e.g., calculation, adsorption analysis, and other procedures). Table 2.2 shows some surface area determinations made for different clay minerals using absorption of water, cetyl pyridinium bromide (CPB), or N_2 gas. Not only were large differences observed between the different mineral specimens, but also between the different experimental methods.

Table 2.2 Specific surface areas determined for selected clay minerals (Source: Tim, 1992)

	Total surface area (m^2/g)		
	H_2O method	CPB method	N_2 gas method
Montmorillonite	300	800	784
Mica-smectite (interstratified)	57	152	109
Kaolinite	17	15	32
Allophane	484	0	157

2.4.2 Origin of negative charges on clays

Phyllosilicate minerals usually contain negatively charged layers, which allow cation exchange reactions. The two major sources of these negative charges are described in the following paragraphs.

1. Isomorphous substitution

Isomorphous substitution is a major source of negative charge in 2:1 layer clays. Some of the silicon in the tetrahedral sheet can be replaced by ions of similar size, usually Al^{3+}, but sometimes Fe^{3+} or other ions. Similarly Al in the octahedron sheet may be replaced by Mg^{2+} or Fe^{2+} without disturbing the crystal structure. The resulting negative charge is considered a permanent charge, since it will not change with changing pH. But where it involves transition metal ions it can be increased or decreased by redox reactions.

2. Dissociation of exposed hydroxyl groups

The presence of OH groups on crystal edges or on exposed planes, can give rise to pH sensitive charges. These hydroxyl groups can dissociate, especially at high pH, and the surface of the clay is left with the negative charge of the oxygen ions. This mechanism is important for 1:1 layer silicates, and iron and aluminum oxide clays. Although kaolinite also has sub-basal hydroxyl groups, the negative charges that can be generated from these groups are relatively small.

The exposed OH groups can also adsorb or gain protons. This process, important only in strongly acidic media, creates positive charges, which can be important for the adsorption of anions. The reactions for dissociation and association of protons can be illustrated as follows:

Alkaline medium $\quad -Al\text{-}OH + OH^- \longrightarrow -Al\text{-}O^- + H_2O$

Acidic medium $\quad -Al\text{-}OH + H^+ \longrightarrow -Al\text{-}OH_2^+$

2.5 Characterisation of clay minerals

In recent years, there has been increasing interest in utilizing clay minerals such as bentonite, kaolinite, diatomite and Fullers earth for their capacity to adsorb not only inorganic but also organic molecules. Their low cost and high abundance in most areas of the world, combined with high sorption properties and potential for ion exchange, make these attractive materials to be used as substitutes for activated carbon adsorbents in a wide range of industries.

The physical and chemical properties of these minerals vary appreciably with their compositions making detailed characterisation necessary for understanding their applications. There are many techniques available for mineral characterization, but the most-commonly used tools are X-ray powder diffraction (XRD), X-ray fluorescence (XRF), Fourier transform infrared spectroscopy (FTIR), scanning electron microscopy (SEM), transmission electron microscopy (TEM), differential thermal analysis (DTA), thermo gravimetric analysis (TGA), nuclear magnetic resonance (NMR), electron paramagnetic resonance (EPR), specific surface area and pore volume measurement (BET method), and surface charge density (P_{ZC}) calculation. However, other tools have also been used in the past, and the new methods are being developed, so this is a fluid area in clay mineral studies.

XRD and SEM are the principal methods used to study mineral morphology and crystal structure. Mineral phases are identified by XRD, which also provides information on their crystallinities. The morphology of aggregates is determined by SEM.

TEM is used to study the shapes of individual crystals and their compositions.

XRF investigates the chemical composition of clay minerals.

The FTIR method investigates the vibration frequencies of individual functional groups in minerals, and provides detailed information on -OH, H_2O, Si-O and Al-O groups etc.

NMR spectroscopy is able to determine the distribution of Al between octahedral and tetrahedral coordination, and also the distribution of next-nearest-neighbour environments for individual Si atoms in the tetrahedral sheet.

THE NATIONAL RESEARCH COUNCIL OF THAILAND
RESEARCH LIBRARY

The National Research Council of Thailand
Research Library
Date 26 DEC 2012
Record No. E 42165
Call No.

EPR is used to provide information on the nature and distribution of paramagnetic transition metal ions and on free radical defects within mineral structures.

DTA and TGA are used to determine the mechanisms through which water molecules are lost from clay mineral structures.

The BET method is used to investigate specific surface area, pore volumes and pore diameters of clay minerals. These results along with calculations of the surface charge density (P_{ZC}) can then be related to the clay surface properties.

However, clay mineral identification and characterisation is not an easy task; several clay minerals are closely related, and they are often interstratified with each other. It is, therefore, necessary to use several independent methods for clay analysis and clay mineral quantification in order to have a strong foundation for understanding their properties.

In the present work, the various techniques that have been used for characterisation of the natural and modified kaolin samples are XRD, XRF, FTIR, SEM, and EPR. Specific surface area, pore volume, and pore diameter were also determined by the BET method and the surface charge density (P_{ZC}) was also determined. In the following section, a brief overview of each technique will be described.

2.5.1 X-ray Diffraction (XRD)

X-rays are electromagnetic radiation with wavelengths of about 1 Å (10^{-10} m), which is about the same size as atomic distances in solid. The XRD technique has been in used in two main areas of science, for fingerprint identification of crystalline materials, and for determination of structures. Each crystalline solid has its unique characteristic X-ray powder pattern which may be used as a fingerprint for its identification. Once the material has been identified, X-ray crystallography may be used to determine its structure, i.e. how the atoms pack together in the crystalline state, and to determine interatomic distances and angles. It is also the most fundamental tool used in the identification and characterisation of crystalline clay minerals. It is, however, of less

value in identifying poorly-crystalline phases, especially when present in specimens as only minor components.

As mentioned above, X-rays are electromagnetic radiation with typical photon energies in the range of 100 eV - 100 keV. For diffraction applications, only short wavelength X-rays (hard X-rays) in the range of a few angstroms to 0.1 Å (1 keV - 120 keV) are used. They are produced generally by either X-ray tubes or synchrotron radiation. In an X-ray tube, which is the primary X-ray source used in laboratory instruments, X-rays are generated when electrons emitted from the cathode filament with kinetic energies in the keV range and above attack matter on an anode plate. The anode plate, made from a specific metal of high purity, is typically fabricated from copper, chromium, or another metal as listed in Table 2.3.

Table 2.3 Metals used as anodes for x-ray tubes with characteristic wavelengths λ, typical K_β filter materials, and their appropriate K-edge wavelengths λ_{K^*} (Source: Maslen et al., 1992)

Target Element	Z	λ (nm)				K_β filter	λ_{K^*} (nm)
		$K_{\alpha 1}$	$K_{\alpha 2}$	K_{α}-	K_β		
Cr	24	0.228975	0.229365	0.22909	0.20849	V	0.2269
Fe	26	0.193631	0.194002	0.19373	0.17567	Mn	0.1896
Co	27	0.178900	0.179289	0.17905	0.16208	Fe	0.1744
Ni	28	0.165794	0.166178	0.16591	0.15002	Co	0.1608
Cu	29	0.154059	0.154441	0.15418	0.139225	Ni	0.1488
Mo	42	0.709317	0.713607	0.7107	0.63230	Zr	0.6889
Ag	47	0.559422	0.563813	0.5608	0.49708	Rh	0.5339

*From various tables of the *International Tables for Crystallography*, Vol. C, Section 4.2.2.

The electron current comprises a continuous part, called Bremsstrahlung, and some discrete lines indicative of the chemical elements of the target material. The electron current between filament and anode may be adjusted by tuning the filament current in the 10 mA range. When impinging upon the anode, the electrons are decelerated by their interaction with the target plate atoms, and this leads to the emission of X-rays.

The acceleration voltage (in kV) must be greater than the energy of the characteristic radiation required by the experiment (in keV).

The anode material is often copper to make use of the characteristic Cu Kα line, whose wavelength is 0.154 nm, which is equivalent to 8.04 keV. Other X-ray tubes may be used if the diffraction pattern has to be contracted or expanded or if the excitation of X-ray fluorescence from the sample is to be avoided. A good example of the latter is Fe-containing samples which produce a strong background when Cu Kα radiation is used. The process of impact ionization and relaxation of an X-ray emitting atom is shown schematically in Figure 2.5

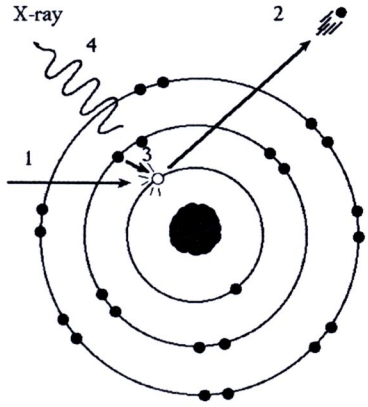

Figure 2.5 Emission of X-rays by an atom through sequential processes of electron impact (1) ionization (2) and simultaneous electronic relaxation (3),and emission of radiation(4). (Ozard, 2006)

In this continuous process, bound electrons are first released and subsequently an electron from a higher energy level relaxes into the vacant state. The relaxation is associated with the emission of radiation, the energy of which corresponds to the energy difference between the final and initial state. This energy thus depends sensitively on the chemical nature of the emitting atom. According to the levels involved, the relaxation of the emitted radiation is denoted by $K_{\alpha 1}$, $K_{\beta 2}$, L_{α}, etc. In most x-ray scattering experiments only the characteristic emission lines are of interest.

The characteristic X-rays are labeled as K, L, M or N to denote the shells they originated from (Figure 2.6). Another designation alpha (α), beta (β) or gamma (γ) is

made to mark the X-rays that originated from the transitions of electrons from higher shells. Hence, a K_α X-ray is produced from a transition of an electron from the L to the K shell, and a K_β X-ray is produced from a transition of an electron from the M to a K shell, etc. Since within the shells there are multiple orbits of higher and lower binding energy electrons, a further designation is made as $\alpha 1$, $\alpha 2$ or $\beta 1$, $\beta 2$, etc. to denote transitions of electrons from these orbits into the same lower shell.

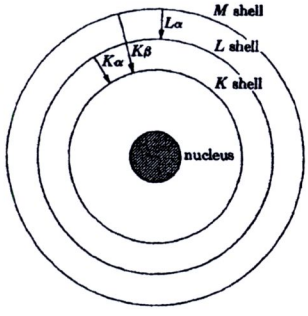

Figure 2.6 Schematic of electronic transition in X-ray emission process.(Cullity, 1956)

In the majority of cases investigations are performed with K_α radiation, because of its higher intensity compared to K_β. A closer look at the K_α radiation reveals its doublet nature. The doublet resolution increases for Bragg peaks with increasing scattering angle 2θ. The K_β line may severely disturb the interpretation of the diffraction pattern and various techniques are applied for its suppression. Very common are edge filters that are introduced into the incident beam path and make use of the fact that the photoionization of deep levels requires a certain minimum energy. In the case of copper, E (Cu $K_{\beta 1}$) = 8.9 keV, and thus a thin Ni foil can be used as an edge filter that significantly suppresses the K_β line. Other foil materials for other tubes are presented in Table 2.3

Diffraction effects are observed when electromagnetic radiation interacts with periodic structures with geometrical variations on the length scale of the wavelength of the radiation. The interaction of the incident rays with the sample produces constructive interference (and a diffracted ray) when conditions satisfy Bragg's law (Figure 2.7).

$$n\lambda = 2d\sin\theta$$

where λ is wavelength of x-ray used, θ is angle between incident x-rays and plane of crystal, *d* is distance between planes of particles, *n* is an integer (1,2,3...) that represents serial order of diffracted beams,

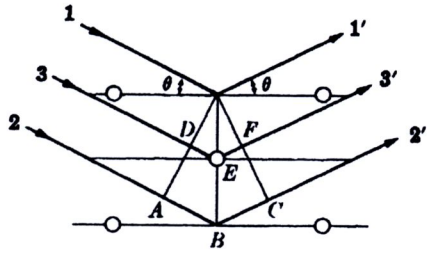

Figure 2.7 Schematic X-ray diffraction interact to plane of sample. (Cullity,1956)

The Bragg law relates the wavelength of electromagnetic radiation (λ) to the diffraction angle (θ) and the lattice spacing in a crystalline sample (*d*). These diffracted X-rays (diffractogram) are then detected, processed and counted. By scanning the sample through a range of 2θ angles, all possible diffraction directions of the lattice should be attained due to the random orientation of the powdered material. Conversion of the diffraction peaks to d-spacings allows identification of the mineral because each mineral has a set of unique d-spacings. Typically, this is achieved by comparison of d-spacings with standard reference patterns for example as illustrated in Figure 2.8.

PDF#33-1161 (Deleted Card): QM = Star (+); d = Diffractometer, I = Diffractometer — PDF Card

Quartz, syn
SiO2

Radiation = CuKa1 — Lambda = 1.540598 — Filter =
Calibration = Internal (Si) — d-Cutoff = — I/Ic (RIR) = 3.6
Ref = Natl. Bur. Stand. (U.S.) Monogr. 25, 18 61 (1981)

Hexagonal—(Unknown), P3221(154) — Z = 3 — mp =
Cell = 4.9134 × 5.4053 — Pearson = hP9 (O2 Si)
Density (c) = 2.649 Density (m) = 2.656 Mwt = 60.08 Vol = 113.01 — F(30) = 76.8 (.0126,31)
Ref = Ibid.

NOTE: Sample from the Glass Section at NBS, Gaithersburg, MD, USA, ground single-crystals of optical quality. To replace 5-490 and validated by calculated pattern. Plus 6 additional reflections to 0.9089. Pattern taken at 25 C. Pattern reviewed by Holzer, J., McCarthy, G., North Dakota State Univ., Fargo, ND, USA, ICDD Grant-in-Aid (1990). Agrees well with experimental and calculated patterns. Deleted by 46-1045, higher F#N, more complete, LRB 1/95.

Color: Colorless

Strong Line: 3.34/X 4.26/2 1.82/1 1.54/1 2.46/1 2.28/1 1.37/1 1.38/1 2.13/1 2.24/1

39 Lines, Wavelength to Compute Theta = 1.54056A (Cu), 1%-Type = (Unknown)

#	d(A)	I(f)	h	k	l	2-Theta	Theta	1/(2d)	#	d(A)	I(f)	h	k	l	2-Theta	Theta	1/(2d)
1	4.2570	22.0	1	0	0	20.850	10.425	0.1175	21	1.2285	1.0	2	2	0	77.660	38.830	0.4070
2	3.3420	100.0	1	0	1	26.651	13.326	0.1495	22	1.1999	2.0	2	1	3	79.875	39.938	0.4167
3	2.4570	8.0	1	1	0	36.541	18.271	0.2035	23	1.1978	1.0	2	2	1	80.044	40.022	0.4174
4	2.2820	8.0	1	0	2	39.455	19.727	0.2191	24	1.1843	3.0	1	1	4	81.145	40.572	0.4222
5	2.2370	4.0	1	1	1	40.283	20.141	0.2235	25	1.1804	3.0	3	1	0	81.470	40.735	0.4236
6	2.1270	6.0	2	0	0	42.464	21.232	0.2351	26	1.1532	1.0	3	1	1	83.818	41.909	0.4336
7	1.9792	4.0	2	0	1	45.808	22.904	0.2526	27	1.1405	1.0	2	0	4	84.969	42.484	0.4384
8	1.8179	14.0	1	1	2	50.139	25.070	0.2750	28	1.1143	1.0	3	0	3	87.461	43.731	0.4487
9	1.8021	1.0	0	0	3	50.610	25.305	0.2775	29	1.0813	2.0	3	1	2	90.855	45.428	0.4624
10	1.6719	4.0	2	0	2	54.867	27.434	0.2991	30	1.0635	1.0	4	0	0	92.819	46.410	0.4701
11	1.6591	2.0	1	0	3	55.327	27.663	0.3014	31	1.0476	1.0	1	0	5	94.662	47.331	0.4773
12	1.6082	1.0	2	1	0	57.236	28.618	0.3109	32	1.0438	1.0	4	0	1	95.115	47.558	0.4790
13	1.5418	9.0	2	1	1	59.947	29.973	0.3243	33	1.0347	1.0	2	1	4	96.223	48.112	0.4832
14	1.4536	1.0	1	1	3	63.999	32.000	0.3440	34	1.0150	1.0	2	2	3	98.734	49.367	0.4926
15	1.4189	1.0	3	0	0	65.759	32.879	0.3524	35	0.9898	1.0	4	0	2	102.195	51.098	0.5052
16	1.3820	6.0	2	1	2	67.748	33.874	0.3618	36	0.9873	1.0	3	1	3	102.556	51.278	0.5064
17	1.3752	7.0	2	0	3	68.128	34.064	0.3636	37	0.9783	1.0	3	0	4	103.880	51.940	0.5111
18	1.3718	8.0	3	0	1	68.321	34.160	0.3645	38	0.9762	1.0	3	2	0	104.195	52.098	0.5122
19	1.2880	2.0	1	0	4	73.460	36.730	0.3882	39	0.9636	1.0	2	0	5	106.141	53.071	0.5189
20	1.2558	2.0	3	0	2	75.668	37.834	0.3982									

Figure 2.8 PDF card (standard pattern card) of quartz (SiO_2) using Cu $K_{\alpha 1}$ as radiation source with wavelength 1.540598 Å.

In the present studies, the sample was rotated within the desired angle and the diffraction intensity and the diffraction angle were measured. Copper metal was used as the X-ray source.

2.5.2 X-ray fluorescence (XRF)

X-ray fluorescence (XRF) is the emission of characteristic "secondary" (or fluorescent) X-rays from a material that has been excited by bombarding it with high-energy X-rays or gamma rays. The phenomenon is widely used for elemental analysis and chemical analysis, particularly in the investigation of metals, glass, ceramics, and building materials, and for research in geochemistry, forensic science, and archaeology.

When a primary X-ray excitation source from an X-ray tube or a radioactive source interacts with a material, the X-ray can either be absorbed or scattered. In the absorption process, if the primary X-ray had sufficient energy, bound electrons are first released, and subsequently an electron from a higher energy level relaxes into the emptied state. The relaxation is associated with the emission of radiation, the energy of which corresponds to the energy difference between the final and initial state. This energy thus depends sensitively on the chemical nature of the emitting elemental atom. Each element has a unique set of energy levels, and thus produces X-rays at a unique set of energies. By determining the energy (wavelength) of the X-ray emitted by a particular element using the Bragg equation, it is possible to determine the identity of that element in samples.

For a particular energy (wavelength) of fluorescent light emitted by an element, the number of photons per unit time (generally referred to as peak intensity or count rate) is related to the amount of that element in the sample. Therefore, by determining the energy of the X-ray peaks and by calculating the count rate (intensity of the various elemental peaks, it is possible to qualitatively establish the elemental composition and to quantitatively measure the concentration of these elements in samples.

The fluorescent radiation can be analysed either by sorting the energies of the photons (energy-dispersive analysis), or by separating the wavelengths of the radiation (wavelength-dispersive analysis). In energy dispersive analysis, the fluorescent x-rays emitted by the material sample are directed into a solid-state detector which produces a "continuous" distribution of pulses, the voltages of which are proportional to the incoming photon energies. This signal is processed by a multichannel analyser (MCA) which produces an accumulating digital spectrum that can be processed to obtain the analytical data. In wavelength dispersive analysis, the fluorescent X-rays emitted by the sample are directed into a diffraction grating monochromator. The diffraction grating is usually a single crystal. By varying the angle of incidence and take-off on the crystal, a single X-ray wavelength can be selected. The wavelength obtained is given by the Bragg's equation.

In wavelength dispersive analysis, the single-wavelength radiation produced by the monochromator is passed into a photomultiplier, a detector similar to a Geiger counter,

which counts individual photons as they pass through. The counter is a chamber containing a gas that is ionised by X-ray photons. A central electrode is charged at (typically) + 1700 V with respect to the conducting chamber walls, and each photon triggers a pulse-like cascade of current across this field. The signal is amplified and transformed into an accumulating digital count. These counts are then processed to obtain analytical data.

1. Energy dispersive spectrometry

In energy dispersive spectrometers (EDX or EDS) (Figure 2.9), the detector allows the determination of the energy of the photon when it is detected. Detectors historically have been based on silicon semiconductors, in the form of lithium-drifted silicon crystals, or high-purity silicon wafers.

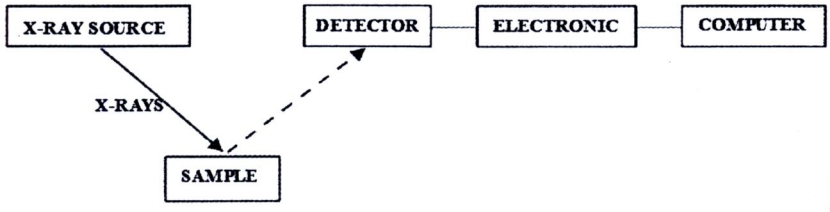

THE NATIONAL RESEARCH COUNCIL OF THAILAND
RESEARCH LIBRARY

Figure 2.9 Schematic arrangement of EDX spectrometer (Shankar, 2009)

2. Wavelength dispersive spectrometry

In wavelength dispersive spectrometers (WDX or WDS), the photons are separated by diffraction on a single crystal before being detected (Figure 2.10). Wavelength dispersive spectrometers are occasionally used to scan a wide range of wavelengths, producing a spectrum plot as in EDS.

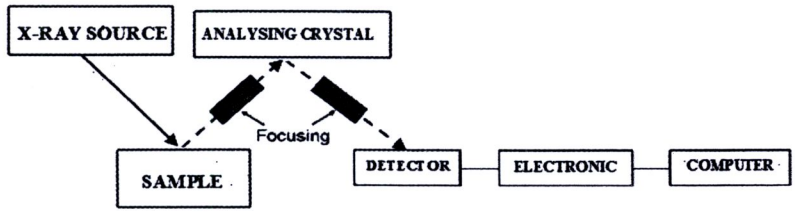

Figure 2.10 Schematic arrangement of WDX spectrometer. (Shankar, 2009)

In the present work, X-ray fluorescence (XRF) analysis was used to determine the major elemental contents of clay samples from Thai kaolins.

2.5.3 Fourier transform infrared (FTIR) spectroscopy

FTIR is an absorption spectroscopic technique that uses the infrared region of the electromagnetic spectrum to measure the energies of vibrations of Chemical groups and molecules. As each functional group or structural characteristic of a molecule has a distinct vibrational signal, this allows a unique spectrum to be generated for any sample that is put in the path of the infrared light.

The infrared portion of the electromagnetic spectrum is divided into three regions; the near-, mid- and far- infrared, named for their relation to the visible spectrum. The far-infrared, approximately 400–10 cm^{-1}(1000–30 μm), lying adjacent to the microwave region, has low energy and may be used for rotational spectroscopy. The mid-infrared, approximately 4000–400 cm^{-1} (30–2.5 μm) is used to study the fundamental vibrations and associated rotational-vibrational structure. The higher energy near-IR, approximately 14000–4000 cm^{-1} (2.5–0.8 μm) can excite overtone or harmonic vibrations. The names and classifications of these subregions are merely conventions. They are neither strict divisions nor based on exact molecular or electromagnetic properties.

Simple diatomic molecules have only one bond, which may stretch. More complex molecules have many bonds, and vibrations can be conjugated, leading to infrared absorptions at characteristic frequencies that may be related to chemical groups. For example, the atoms in a CH_2 group, commonly found in organic compounds can vibrate in six different ways: symmetrical and antisymmetrical stretching, scissoring, rocking, wagging and twisting:

An infrared spectrum is collected by passing a beam of infrared light through a sample. Examination of the transmitted light reveals how much energy was absorbed at each wavelength. This can be done with a monochromatic beam, which changes in wavelength over time, or by using a Fourier transform instrument to measure all wavelengths at once. From this, a transmittance or absorbance spectrum can be produced, showing at which IR wavelengths the sample absorbs. Analysis of these absorption characteristics reveals details about the molecular structure of the sample.

When the frequency of radiation is the same as the vibrational frequency of a bond, absorption occurs.

This technique works almost exclusively on samples with covalent bonds. Simple spectra are obtained from samples with few IR active bonds and high levels of purity. More complex molecular structures lead to more absorption bands and more complex spectra. However, the technique has been highly successful for applications in both organic and inorganic chemistry, and it has also been used successfully in the characterisation of semiconductors, such as silicon, gallium arsenide, gallium nitride, zinc selenide, amorphous silicon, silicon nitride, etc.

Infrared spectral analysis has been used to characterize clays for many years (e.g. Farmer, 1964). This method is somewhat less sensitive to differences in clay structures and as a result its use as a method of identification, especially in a mixed-phase sample, is difficult. However, the method is valuable for identifying features of pure phases, especially when these have been subjected to prior identification by XRD.

The clay structure absorbs IR radiation according to the vibration frequencies of its various crystalline components. These range from the OH unit through the SiO_4 and AlO_4 tetrahedral units, the AlO_6, MgO_6, FeO_6, etc., octahedral units to complex, multi-atomic portions of the silica sheet network. The most useful zones of infrared analysis for clay minerals are in the OH vibrational region, because here one can have access to information not available from other analytical methods.

In recent years attenuated total reflection (ATR) infrared spectroscopy has become widely used in geological applications. This method takes advantage of the difference in refractive index between the sample being measured and a high-refractive index crystal such as ZnSe, Ge, or diamond. The sample is placed in contact with the crystal, and modulated infrared light from a Fourier Transform Infrared (FTIR) interferometer is allowed to enter the crystal. The light then penetrates into the sample via an "evanescent wave." Specific frequencies of the in-coming radiation, corresponding to the fundamental vibrational frequencies, vibrational overtones of the sample material are absorbed, and the rest of the light is reflected through the crystal and into a detector. This powerful technique has become a potentially useful mineral analytical tool for a

wide range of investigations, and has brought appreciable advances in the geosciences (see e.g. Figure 2.11).

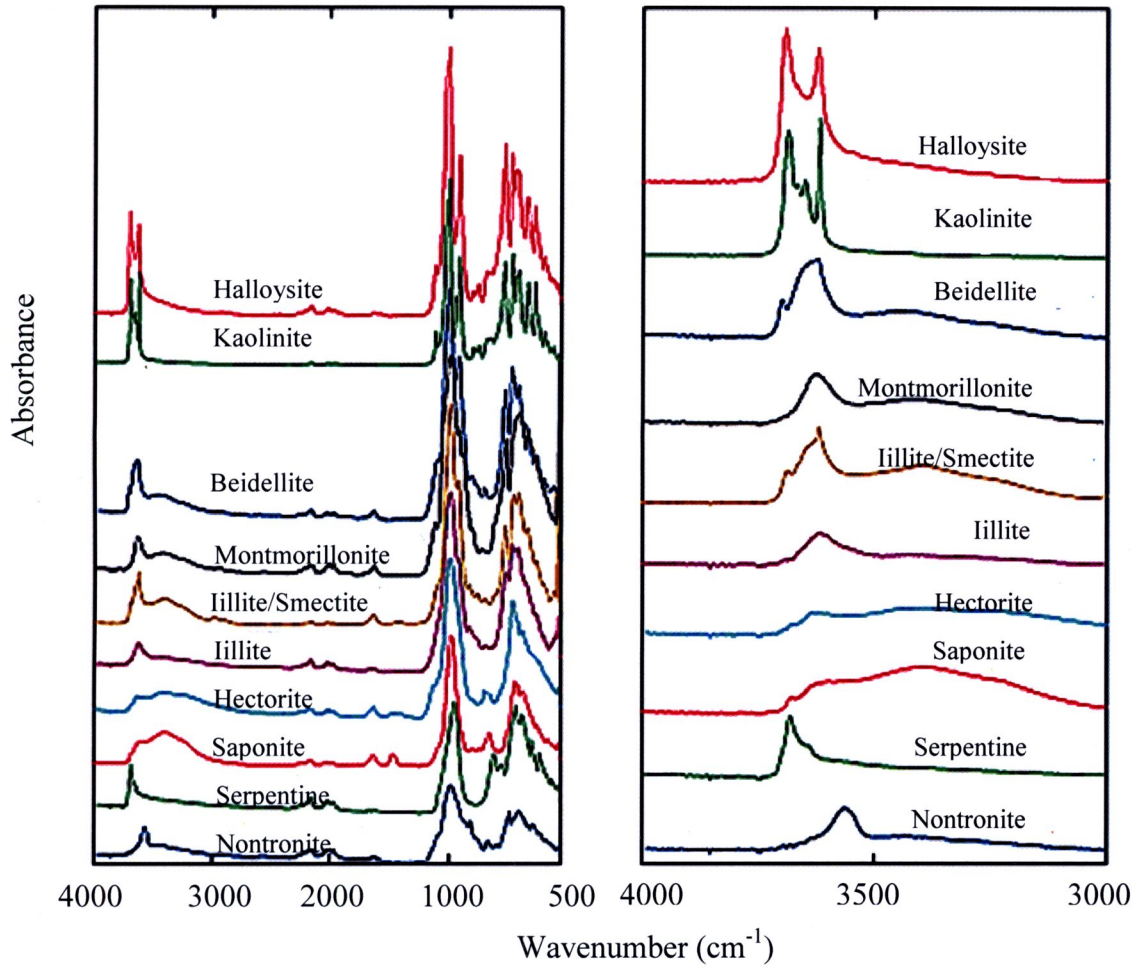

Figure 2.11 ATR spectra of clay minerals. Spectra covering the full available wavenumber range (a) and (b)same spectra, zoomed into the 3000-4000 cm^{-1} to emphasize the variability of the hydration overton. (Glotch et al., 2007)

2.5.4 Scanning Electron Microscopy (SEM)

The scanning electron microscope (SEM) has become one of the most widely utilized instruments for materials characterisation. This technique is a microscope that uses a focused beam of high-energy electrons to generate a variety of signals at the surface of solid specimens (Figure 2.12). The electrons interact with the atoms that make up the sample producing signals that contain information about the sample's surface topography, morphology, composition and other properties, such as electrical conductivity. The SEM is also capable of performing analyses of selected point

locations on the sample; this approach is especially useful in qualitatively or semi-quantitatively determining chemical compositions (using EDS), crystalline structure, and crystal orientations (using EBSD).

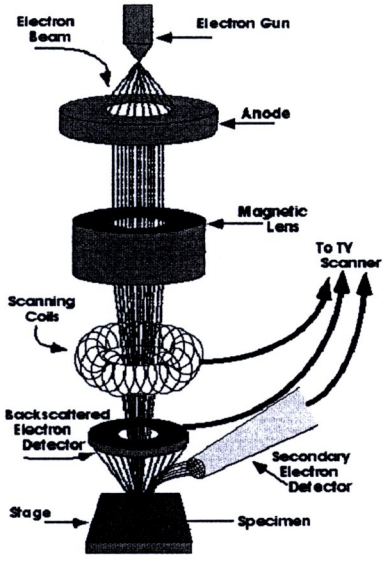

Figure 2.12 Schematic arrangement of a scanning electron microscope. (Schweitzer, 2011)

The SEM is an instrument that produces a largely magnified image by using electrons instead of light to form an image. A beam of electrons is produced at the top of the microscope by an electron gun. The electron beam follows a vertical path through the microscope, which is held in a vacuum. The beam travels through electromagnetic fields and lenses, which focus the beam down toward the sample. Once the beam hits the sample, electrons and X-rays are ejected from the sample (Figure 2.13). Detectors collect these X-rays, backscattered electrons, and secondary electrons and convert them into a signal that is sent to a screen similar to a television screen, where the final image is produced.

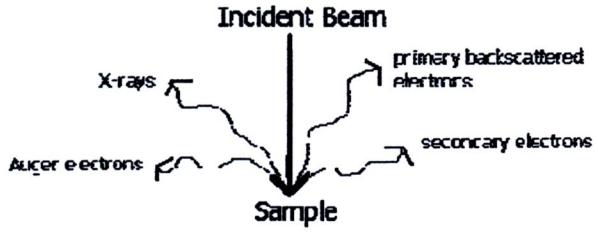

Figure 2.13 Schematic of the interaction between the incident beam and the sample (Schweitzer, 2011)

Because SEM utilizes vacuum conditions and uses electrons to form an image, special sample preparation must be performed. All water must be removed because this would vaporize in the vacuum. Although all metals are conductive and require no prior preparation, non-conductors must be made conductive by covering the sample with a thin layer of conductive material. This is done by using a device called a sputter coater.

The sputter coater uses an electric field and argon gas. The sample is placed in a small chamber under vacuum. Argon gas and an electric field cause an electron to be removed from the argon, making the atoms positively charged. The argon ions then become attracted to a negatively charged gold foil. The argon ions knock gold atoms from the surface of the gold foil, and these then fall and settle onto the surface of the sample producing a thin gold coating.

Even though several techniques have been used to study clay minerals, SEM is a very important. For example it can distinguish between kaolinite and halloysite minerals that produce almost identical XRD and FTIR patterns, on the basis of their individual morphologies. These are hexagonal plates for kaolinite, whereas halloysite has a tubular shape. Thus the SEM technique is of great importance in discriminating the various kaolin-group minerals that have been investigated in the present project.

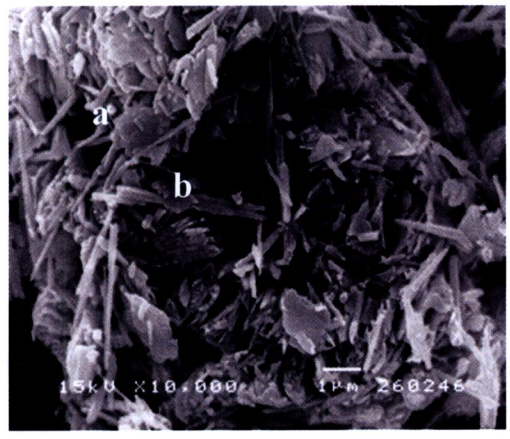

Figure 2.14 SEM images illustrate the morphology of Ranong kaolin minerals, (a) the hexagonal shape of kaolinite, and (b) the tubular shape of halloysite.

In this work SEM was used to investigate morphology of kaolin samples (e.g. Figure 2.14) with magnifications of 5,000, 10,000 and 20,000.

2.5.5 Electron paramagnetic resonance (EPR) spectroscopy

EPR, also known as ESR spectroscopy is a techniquethat is able to provide information specifically on the chemical environments of unpaired electrons in molecules such as free radicals and paramagnetic transition metal complexes. Since its first experimental demonstration in 1944, application of EPR spectroscopy have progressed steadily through physics through physics, biology, chemistry, biochemistry, medicine and into food science.

The principles underlying EPR spectroscopy closely resemble those of the more familiar NMR spectroscopy, except that EPR depends on interactions between unpaired electrons and an external magnetic field, B_O. An unpaired electron, by virtue of its spin, possesses a magnetic moment, which produces two spin states when it interacts with a magnetic field (known as the electronic Zeeman effect). The energies of these states are equal to $g\mu_B B_o m_s$, where m_s is the electron spin quantum number, μ_B is the Bohrmagneton (9.27×10^{-24} J/T), and g is a constant specific to the molecule containing the unpaired electron (commonly referred to as the g-factor or the g-value). For a single unpaired electron, m_s has the values ±½ and the separation of the two spin energy levels is $\Delta E = g\mu_B B_o$. Resonance between the electron energy states can be achieved by

absorption of electromagnetic radiation in the microwave energy range. Thus $h\upsilon = \Delta E$, where h is the Planck's constant (6.62607×10^{-24} Js) and υ is the microwave frequency (Figure 2.15). The microwave sources most commonly used for EPR spectroscopy emit radiation at ~9.6 GHz, known as X-band, and the magnetic field for resonance of a free electron is thus around 340 mT.

There are several other microwave frequency bands now available, the most important being L- (1 GHz), S- (3.5 GHz), K-(24 GHz), Q- (35 GHz), and W-bands (95 GHz), each with some advantages and disadvantages the others. They will not be discussed in detail in this thesis.

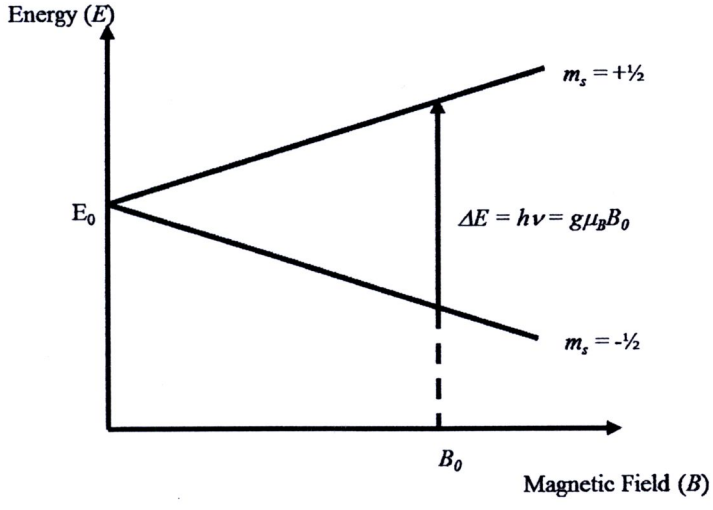

Figure 2.15 The energy state of an electron in a magnetic field and the conditions for observation of electron paramagnetic resonance. (Adapted from Goodman and Raynor, 1970)

However, sensitivity (in terms of the minimum number of electrons detectable per unit weight of sample) increases with increasing frequency, but the working sample size decreases with increasing frequency. The field range over which the EPR signal is dispersed increases with increasing frequency, so the components with different *g*-values are better resolved. On the other hand, inherently broad signals may be unobservable at high microwave frequencies. For samples containing water, there is the problem of absorption of microwaves by water (to generate heat). The total amount of water in a specimen must, therefore, be strictly controlled in EPR spectroscopy and this becomes increasingly more critical at high frequencies. Consequently, there is no

universally ideal frequency for EPR spectroscopy, and X-band is generally accepted is providing the best compromise between the various factors that determine the detection, sensitivity and resolution of EPR spectra from samples containing unpaired electrons.

In the absence of saturation the intensity or the area under the absorption curve is proportional to the number of unpaired electron spins in the sample. Spectra are generally recorded as first derivatives of the absorption curve (Figure 2.16(b)) rather than the absorption curve itself (Figure 2.16(a)) and measurements of intensities, therefore, involve a double integration of the experimental curve. Sometimes it may be informative to record second derivative spectra (Figure 2.16(c)). These provide improved resolution of overlapping peaks and enhance the amplitude of narrow peaks relative to broader ones.

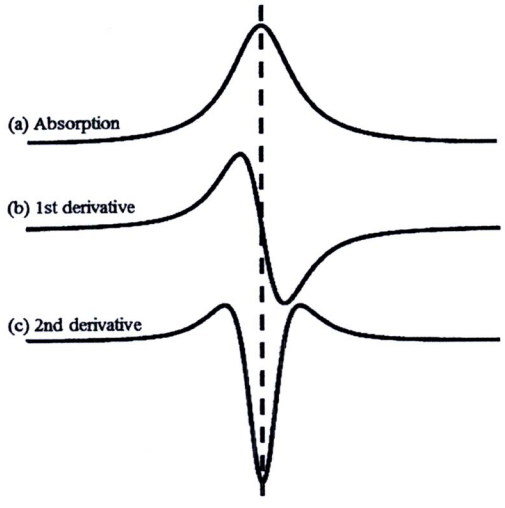

Figure 2.16 A Lorentzian line-shape displayed as (a) absorption curve, (b) first derivative, and (c) second derivative (phase changed by 180° for ease of comparison with absorption shape).(Adapted from Goodman and Raynor, 1970)

EPR spectra are characterised by a number of parameters, the most important of which are the *g*-factor and hyperfine splitting, although the line-shape, line width and power saturation characteristics may also be informative. A close study of these parameters often enables detailed structural information about a particular radical to be deduced.

1. The *g*-value

In a typical EPR experiment, the microwave frequency is held constant and the magnetic field is scanned to find the field, B_O, at which absorption of microwave radiation occurs. The g value is then calculated from the equation in Figure 2.14, i.e. $g = 71.44775\ \upsilon / B_O$, when υ is in GHz and B_O in mT.

The value of g for a free electron is 2.00232, and it is very close to this value for many free radicals which contain only light atoms (i.e. from the 1st row of the Periodic Table). Deviations from the "free spin" g-value occur through a process called spin-orbit coupling, in which coupling occurs between the spin and orbital angular of the unpaired electron in molecular orbitals. This results in the electron having a slightly different magnetic moment from that of a completely free electron and consequently a slightly different resonance energy (i.e. g is dependent on the chemical nature of the paramagnetic species). These differences may not be the same for different directions, if the molecular orbital containing the unpaired electron is non-spherical; this is called g-value anisotropy and the g-value is really a tensor with the diagonal components (g_{xx} g_{yy} g_{zz}). The principal components of the g-tensor correspond to the alignment of the principal axes of the molecular orbital containing the unpaired electron with the direction of the external magnetic field. For molecules with axial symmetry $g_{xx} = g_{yy}$. These are often referred to as $g_\perp$ with g_{zz} as $g_{//}$, and correspond to the alignment of the principal axis of the molecular orbital containing the unpaired electron perpendicular and parallel, respectively, to the direction of the external magnetic field.

With a single crystal, the principal g-values can be determined by measuring EPR spectra as a function of orientation of the sample in the magnetic field, but with powder or frozen solutions all orientations are present simultaneously. The EPR spectra then correspond to the sum of the spectra from all possible orientations. In 1st derivative recordings, the contributions from many orientations cancel out, however, and the resulting spectrum contains features corresponding to the principal values of the g tensor. Simulations of absorption and 1st derivative spectra are shown in Figure 2.17 for molecular species with axial and non-axial symmetry.

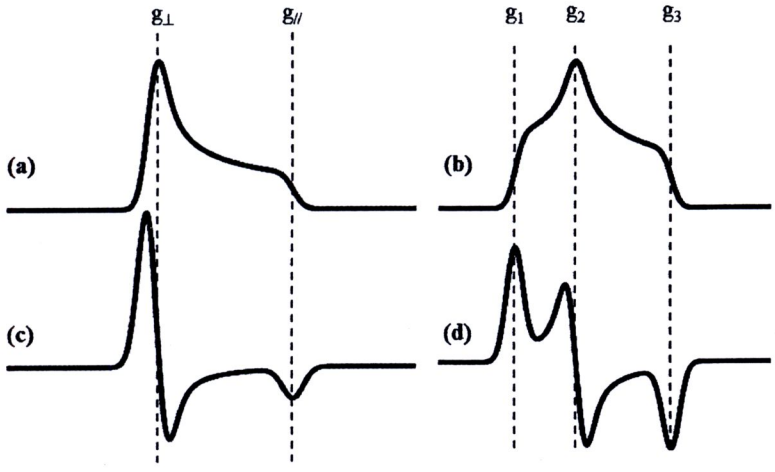

Figure 2.17 Diagram to show the effects of *g*-value anisotropy on the axially (a,c) an non-axially (b,d) symmetrical EPR spectra of powder or frozen solutions samples shown as absorption (a,b) and first derivative (c,d) curves. (Adapted from Goodman and Reynor, 1970)

In fluid solutions, rapid molecular tumbling of the radicals results in an averaging of the anisotropy and a symmetrical spectrum. The *g*-value is then isotropic and is sometimes referred to as g_{iso}.

Deviations of *g*-values from 2.00232 are generally small for organic radicals, for inorganic radicals they are in the range of 1.9 to 2.1, but for *d*-metal complexes, much greater deviations from the free spin value may be observed, especially in complexes with more than one unpaired electron.

2. Hyperfine splitting

If a free radical or other paramagnetic molecule contains nuclei with non-zero spin, I, (e.g. ^{1}H, ^{13}C, ^{14}N, ^{17}O, etc), additional splitting of the electron energy levels occurs as a result of coupling between the electron and nuclear spins. In a hydrogen atom the electron interacts with the proton which has a spin, I, equal to ½. The proton spin has two possible orientations ($m_I = \pm ½$), parallel or antiparallel to the electron spin ($m_S = \pm ½$), so that four energy levels result (Figure 2.18). The nuclear spin quantum number, m_I, does not change during an electronic transition, so there are two allowed transitions, which are indicated by arrows in Figure 2.18. The EPR spectrum of the hydrogen atom, therefore, consists of two peaks of equal intensity. The separation of the lines is known

as the hyperfine splitting, which is given the symbol, a, or sometimes A. Hyperfine splittings are measured from the magnetic field separation and are quoted in millitesla (mT) using the SI system of nomenclature, although many spectrometers still use the gauss. Some workers also use energy (cm^{-1}) or frequency units (MHz) for hyperfine splittings.

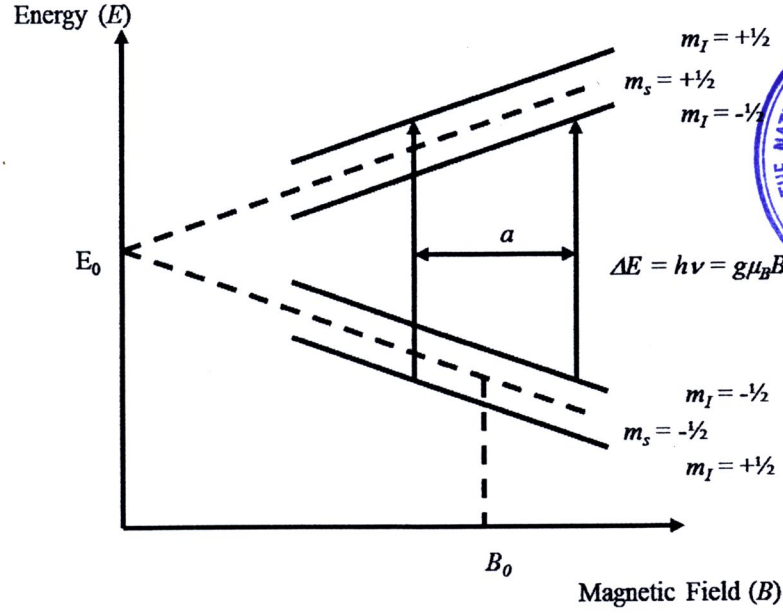

THE NATIONAL RESEARCH COUNCIL OF THAILAND
RESEARCH LIBRARY

Figure 2.18 Splitting of electron energy levels in a magnetic field B in the presence of a nucleus with spin I = ½ . (Adapted from Goodman and Reynor, 1970)

In general, the interaction of the unpaired electron with a nucleus of spin, I, gives hyperfine structure that consists of $2I + 1$ peaks and hyperfine patterns can sometimes be used as fingerprints for the magnetic nuclei. The magnetic properties of some of the most important nuclei that might be encountered in samples in the natural sciences are listed in Table 2.4. The magnitudes of any hyperfine splittings are proportional to the product of the magnetic moment, μ_N, of the nucleus and the fractional occupancy of the molecular orbital containing the unpaired electron by atomic orbitals on that nucleus. Thus for a particular type of nucleus the EPR hyperfine splitting provides information on the unpaired electron density on that nucleus.

Table 2.4 Magnetic properties of some common nuclei with non-zero spin

(Source: Adapted from Goodman and Raynor, 1970)

Isotope	Natural abundant (%)	Magnetic Moment (Nuclear Magneton)	Spin (I)
H-1	99.9844	2.7927	½
H-2	0.0115	0.8574	1
C-13	1.1080	0.7022	½
N-14	99.635	0.4036	1
N-15	0.3650	-0.2830	1/2
O-17	0.0370	-1.8930	5/2
F-19	100.00	2.6273	½
Na-23	100.00	2.2162	3/2
Mg-25	10.05	-0.8547	5/2
Al-27	100.00	3.6385	5/2
Si-29	4.7	-0.5540	½
P-31	100.00	1.1305	½
S-33	0.74	0.6427	3/2
Cl-35	75.4	0.8209	3/2
Cl-37	24.6	0.6833	3/2
K-39	93.08	0.3909	3/2
Ti-47	7.75	-0.7871	5/2
Ti-48	5.51	-1.1022	7/2
V-51	100.00	5.1392	7/2
Cr-53	2.245	-0.4735	3/2
Mn-55	100.00	3.4611	5/2
Fe-57	2.245	0.0903	½
Co-59	100.00	4.6388	7/2
Cu-63	69.09	2.2206	3/2
Cu-65	30.91	2.3790	3/2

As with the *g*-value, the magnitudes of hyperfine splittings vary with orientation of the molecular orbital relative to the magnetic field. The principal values of the hyperfine tensor are referred to as A_{xx}, A_{yy}, A_{zz}, or $A_{\perp}$ and $A_{//}$ if there is axial symmetry. In powder or frozen solution samples, spectra such as those in Figure 2.20, are further split by hyperfine structure. Also, in fluid solutions, rapid tumbling of molecules removes the anisotropy, and just $2I + 1$ symmetrical peaks are observed.

3. Spectral line-shapes, widths, and saturation characteristics

The shapes and widths of the lines in EPR spectra provide information on the factors governing the interaction of the unpaired electron with its environment. The line width is determined primarily by the spin-lattice relaxation time (T_1) and the spin-spin

relaxation time (T_2). The spin-lattice relaxation time is related to the lifetime of the electronic excited state and is governed by the rate of exchange of energy between the excited state electrons and the thermal vibrations of the lattice. It is temperature dependent and represents the time for the recovery of the magnetisation of the paramagnetic system along the applied magnetic field direction after equilibrium has been disturbed. Spin-spin relaxation represents the time taken for oscillating components of the magnetisation in the plane perpendicular to the applied magnetic field to get out of phase with one another, and is largely temperature independent. It is determined by the exchange interactions between the assembly of spins (electronic and nuclear) in the sample. The normal spin-spin dipolar interaction produces a line-shape of a Gaussian form, whereas spin-lattice interactions, or motional averaging effects that occur in solution, give a Lorentzian form. Broadened spectral lines may also be obtained when a sample contains hyperfine structure with splittings less than the line width, or a mixture of components, whose separations are less than their line widths.

In the presence of a magnetic field, the populations N_{gd} and N_{ex} of the ground and excited states (Figure 2.15) are given by the Boltzmann equation,

$$N_{ex} = N_{gd} \exp(-h\upsilon/kT)$$

In an EPR experiment, transitions are induced between these states and new steady state populations n_{gd} and n_{ex} are established. The change in populations between the states is governed by the microwave power absorbed, P_a, and the transition probability, W_e. If n_{gd} and n_{ex} are similar to N_{gd} and N_{ex}, the EPR signal intensity is proportional to the square root of the microwave power, which indicates that the relaxation processes are sufficiently rapid to re-establish the equilibrium population. However as n_{ex} approaches n_{gd}, the rate of signal increase with increasing power slows down, and eventually reaches a maximum; this process is generally referred to as saturation. The value of $P_{1/2}$, which is the microwave power corresponding for half saturation, is a useful parameter for comparing the saturation characteristics of different molecules. Because T_1 is strongly temperature dependent, saturation generally occurs more readily at low temperatures and selection of microwave power needs to be made with care when working with magnetically-dilute free radical samples, where spin-spin relaxation may be inefficient.

4. EPR spectra of Fe (III) and Mn(II) species

The EPR spectra of Fe(III) and Mn(II) species are considered in this section, because of their common occurrence in clay mineral samples. Both ions contain five 3d electrons, and are thus isoelectronic. In the presence of crystals fields, they can exist in states with 1, 3, or 5 unpaired electrons. However, when oxygen atoms are coordinated to the metals, they invariably occur in the high-spin (^{6}S) state (i.e. they have one electron in each of their 3*d* orbitals). Consequently, the other states will not be considered here.

In ions with more than one unpaired electron, there are interactions between the individual electron magnetic moments and the magnetic fields generated by the other electrons. The sextet nature of the free ion ground state remains in the presence of crystal fields of various symmetries, but spin orbit coupling leads to a splitting of the ground state energy levels (called the zero field splitting). These levels are split further in the presence of a magnetic field as a result of interaction with the electron spin angular momentum (Figure 2.19). The right hand side of Figure 2.19 illustrates the five allowed EPR transitions, but these are sensitive to the relative magnitudes of the zero field and electronic Zeeman terms, and consequently are not always observed.

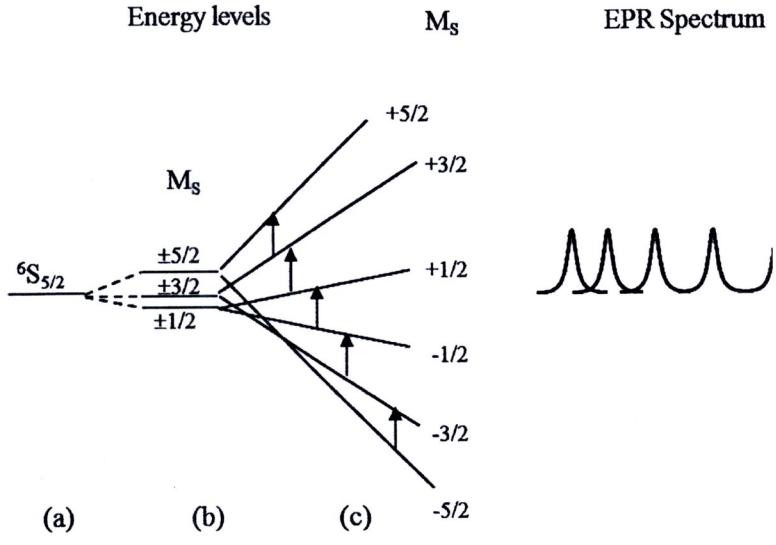

Figure 2.19 Diagrammatic representation of the lowest electronic energy state for high-spin Fe(III) in a crystal field of (a) Oh symmetry, (b) D4h symmetry, with the effects of (c) spin-orbit coupling and (d) external magnetic field.

The zero-field splitting may be anisortropic and is conventionally described by two terms, D and E, where the axis system is defined so that $E \leq D/3$. The positions of the various resonance lines have been calculated as a function of hυ/D, and are illustrated for E = 0 (Figure 2.20), E = D/3 and E = D/4 (Figure 2.21).

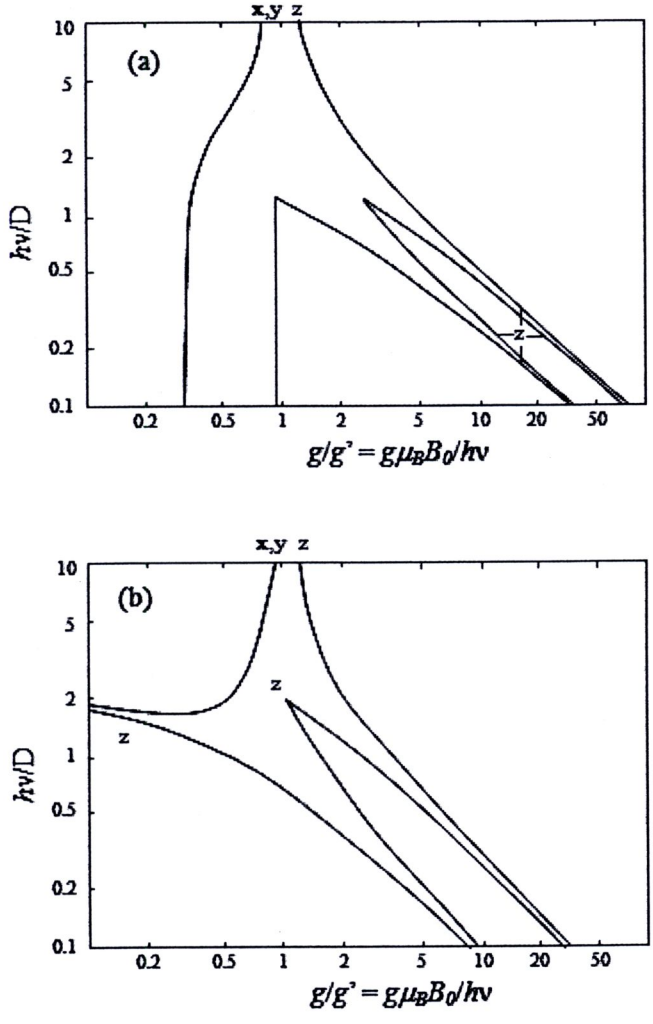

Figure 2.20 Variation as a function of the zero-field splitting, D, of the positions of the a) $m_s(-5/2) \rightarrow m_s(-3/2)$, b) $m_s(-3/2) \rightarrow m_s(-1/2)$, c) $m_s(-1/2) \rightarrow$ ms (+1/2) d) $m_s(+1/2) \rightarrow m_s(+3/2)$, and e) $m_s(+3/2) \rightarrow m_s(+5/2)$ transitions in the EPR Fe(lll) for E = 0

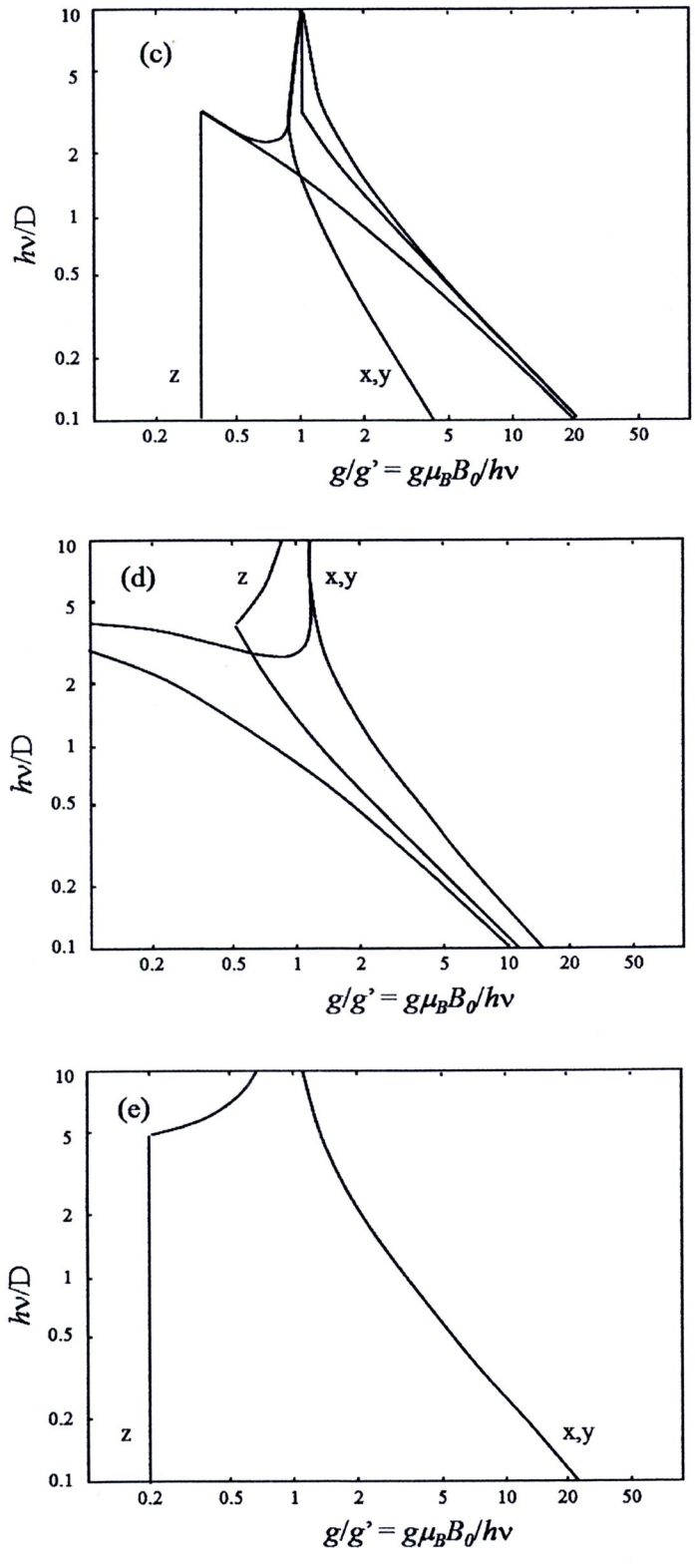

Figure 2.20 (cont'd).

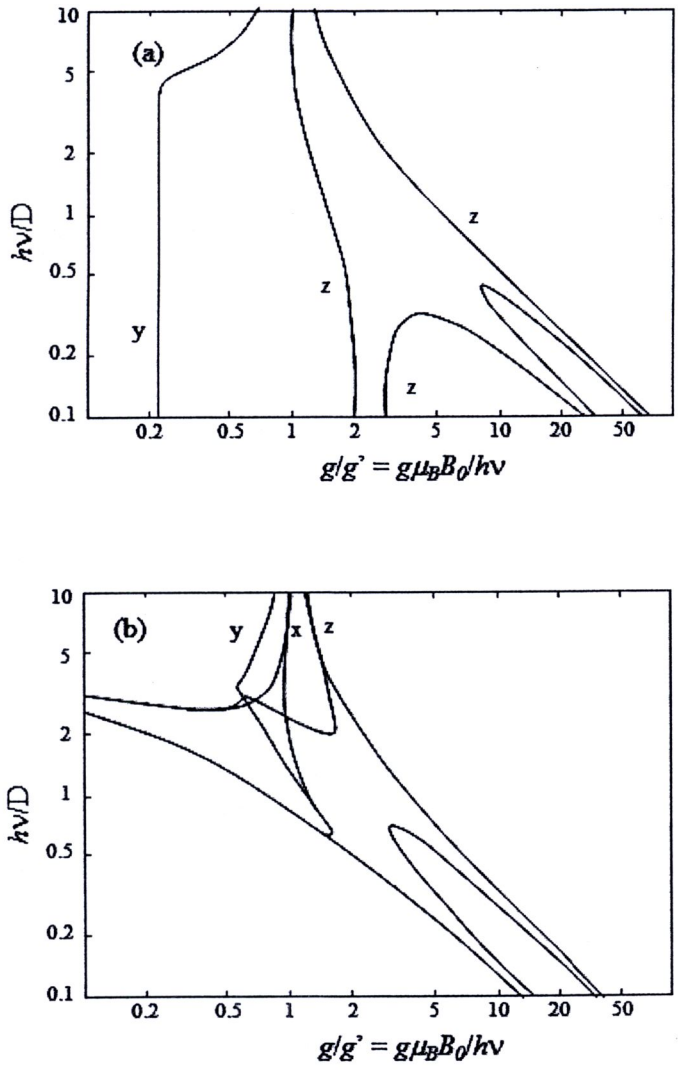

Figure 2.21 Variation as a function of the zero-field splitting, D, of the positions of the (a) $m_s(-5/2) \rightarrow m_s(-3/2)$, and $m_s(3/2) \rightarrow m_s(5/2)$, (b) $m_s(-3/2) \rightarrow m_s(-1/2)$ and $m_s(1/2) \rightarrow m_s(3/2)$, and (c) $m_s(-1/2) \rightarrow m_s(+1/2)$ transitions in the EPR spectra of Fe(III) for E = D/3,and (d) $m_s(-1/2) \rightarrow m_s(1/2)$ transitions in the EPR spectra of Fe (III) for E = D/4

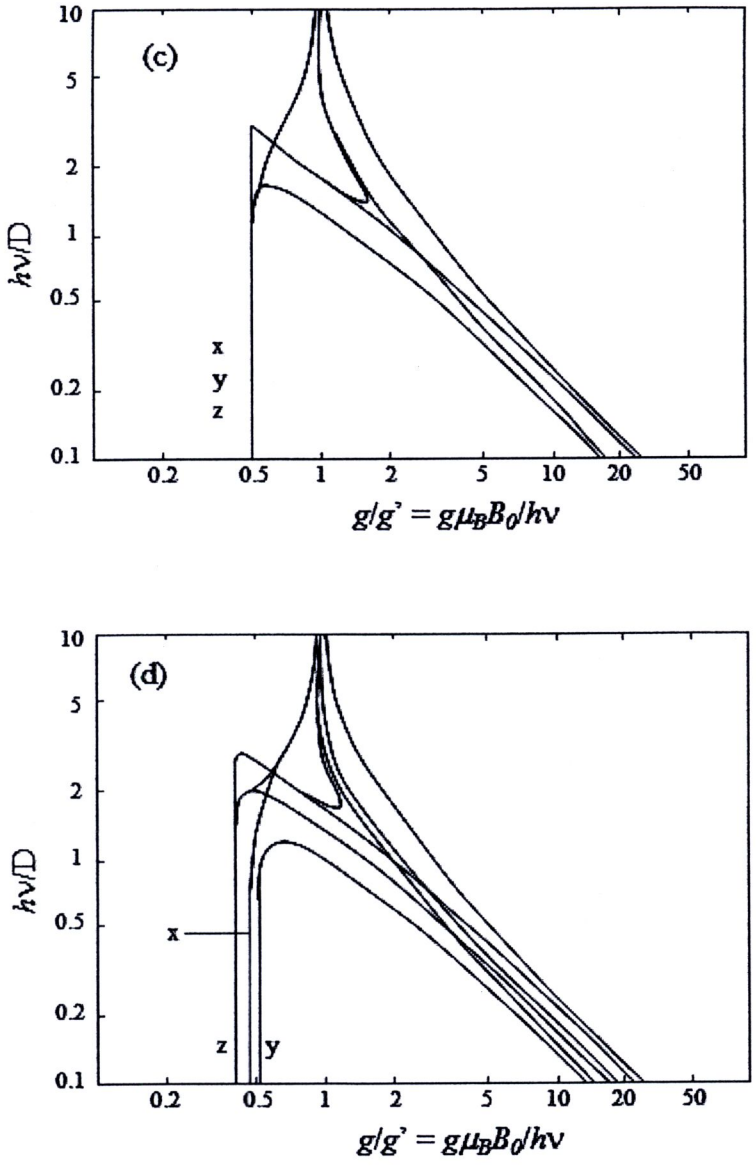

Figure 2.21 (cont'd).

In these plots g is always close to 2.0, but a new parameter, g′, is used to define the apparent g-values that are obtained from experimental peak positions. It is clear from Figures 2.20 and 2.21 that it is only when D is small that the resonance peaks are centred on $g = 2$, the true g-value. The apparent g-value is used to describe the experimental results in this thesis.

In powder or frozen solution samples, EPR spectra consist of a superimposition of peaks covering all molecular orientations. When these are spread over a large energy range, the peak height is very small, and the spectra are dominated by those transitions that are isotropic or near isotropic in character. The fact that peaks with *g*-values close to 4.27 are very common features of the EPR spectra of Fe(III) complexes with organic ligands is not because of any inherent preference of Fe(III) for environments with rhombic or near rhombic symmetry (E/D $\approx$ 0.3), but because of the low level of anisotropy in the $m_s(-1/2) \rightarrow m_s(+1/2)$ transition in this symmetry, Most other transitions in Fe(III) have high degrees of anisotropy and hence extremely large powder spectral line widths and small amplitudes. Two other situations that are revealed by examination of Figures 2.19 and 2.20 as giving powder spectral components with significant intensities are (i) small D, which produces a spectrum centred on $g = 2$, and (ii) large D and zero E, which produces a spectrum with $g_{\perp} = 6$ and $g_{//} = 2$.

Manganese spectra contain sextet hyperfine patterns, which arise from interactions between the unpaired electrons and the ^{55}Mn nucleus, which has I = 5/2 (Table 2.4.), and the observation of such structure is often taken as a fingerprint for the presence of Mn(II). However, similar hyperfine structural patterns would be expected for Mn(IV), which has three 3d electrons, if it is in an environment with (near) cubic symmetry, as would be expected for isomorphous substitution for Si in an aluminosilicate structure.

The discussion so far has assumed that the metal ion is in a magnetically-dilute environment. When magnetic interactions occur between neighbouring ions, dipolar splittings proportional to r^{-3} are produced, where r is the electron- electron separation. If a number of relatively small values of r exist within a specimen, then an envelope of lines rather than a single transition is seen in the EPR spectrum. A diagrammatic representation of various types of EPR spectrum from Fe(III) is given in Figure 2.22.

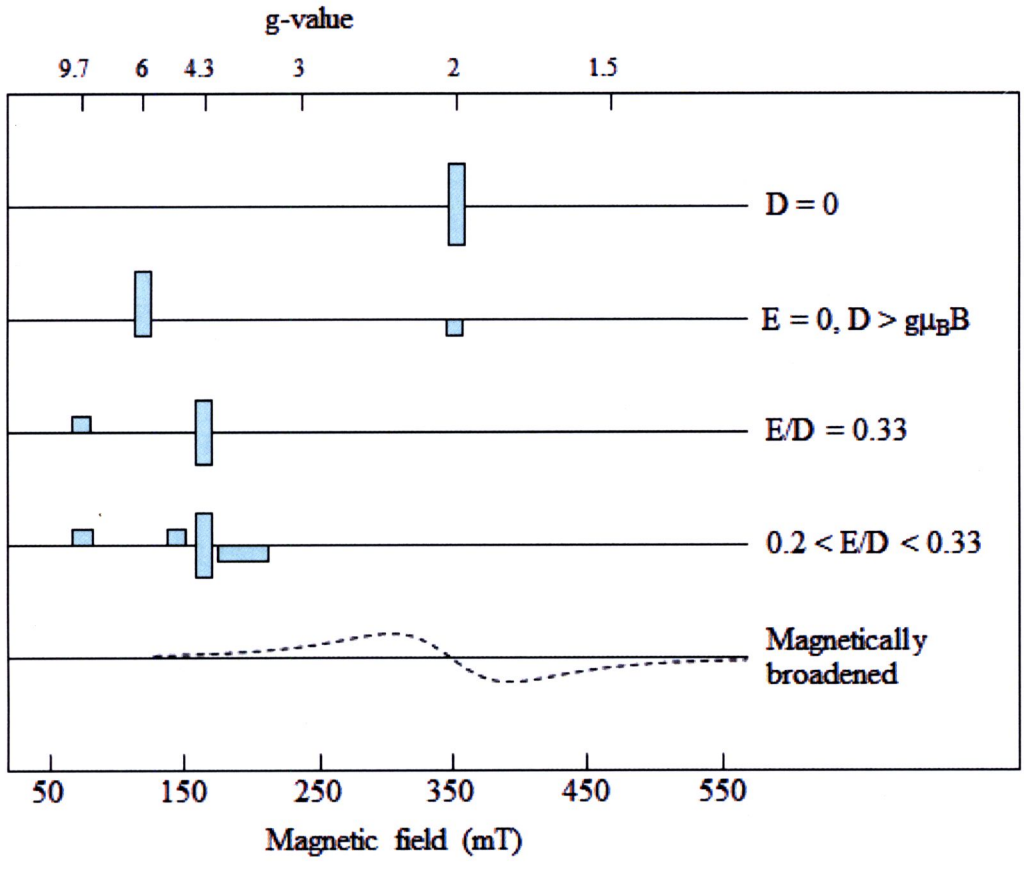

Figure 2.22 Diagrammatic representation of the various types of EPR spectrum for Fe(III) in the high-spin state. (Goodman and Hall, 1994)

5. EPR-spectrometer

An EPR-spectrometer consists of a homogeneous magnetic field, a microwave source, a microwave conductor, a microwave resonator, a detector, an amplifier, and a regulating system. A diagram of a typical EPR-spectrometer is given in Figure 2.23.

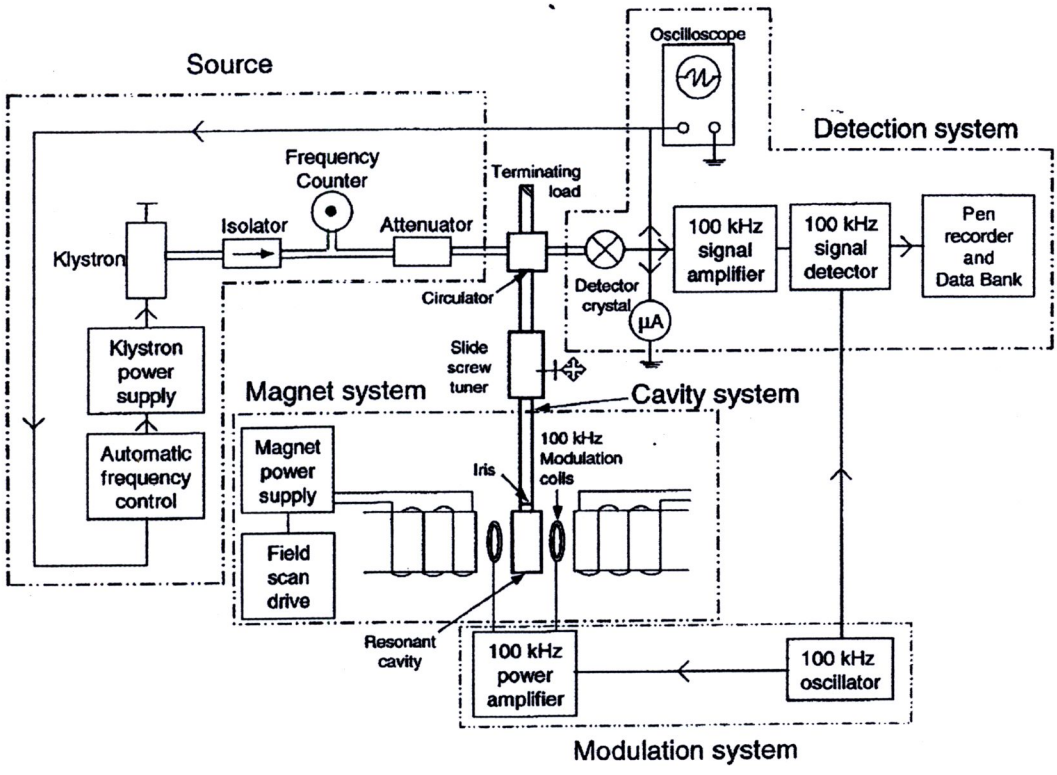

Figure 2.23 Diagram of a typical X-band EPR spectrometer.

The magnetic field is produced by an electromagnet, and microwaves in the EPR spectrometer I used (Bruker EMX, Bruker Biospin, Rheinstetten, Germany) were produced by a Gunn diode. Transmission of the radiation from the source to the resonator as well as to the detector occurs with wavelength conductors. The resonator (cavity) is the part of the microwave conductor where interaction with the sample occurs and where a standing wave is produced. Silicon-diodes are used for detecting the microwave signal.

6. Principle of measurement

The microwave bridge is the core of the spectrometer and the connection between the microwave source and the detector. To receive high signal-to-noise ratios and baseline stability, the magnetic field is modulated at low frequency. Therefore the microwave signal is also modulated with the same frequency and the resulting spectrum is obtained as the 1st derivative of the absorption. In the present work, the best value of the modulation frequency to compromise noise and resolution was 100 kHz.

7. Variable parameters

Some parameters have to be chosen and set independent of the sample before the EPR spectrum can be recorded. The optimum microwave power varies with the temperature at which the spectrum is recorded, and the chemical nature of the signal being investigated, e.g. isolated free radicals often saturate very easily, whereas transition metal ions may resist saturation in spectra recorded at room temperature. The choice of the modulation amplitude is a compromise between the signal height and peak resolution. With decreasing modulation amplitude, resolution is improved, but the peak height is decreased. Another parameter is the receiver gain. It should be chosen to be big enough to obtain a good signal considering that an increasing receiver gain also increases the noise level. The speed of recording one spectrum can be regulated by the conversion time, whereas the time constant filters out noise by slowing down the response time of the spectrometer. The centre field and the sweep width of a spectrum are two other parameters which are adjusted to the sample.

2.5.6 Specific surface area determination using the Brunauer-Emmett-Teller (BET) method

Adsorption is the process of using solids for removing substances from either gaseous or liquid phases. It is simply the preferential partitioning of substances from the gaseous or liquid phase onto the surface of a solid substrate. From the early days of using bone char for decolorisation of sugar solutions and other foods, to the later implementation of activated carbon for removing nerve gases from battlefields, to today's thousands of applications, the adsorption phenomenon has been a useful tool for purification and separation.

The capacity for adsorption of an adsorbent depends on several factors, such as specific surface area, total pore volume, average pore diameter, the porous structure, the surface functionality and ion exchange capacity, etc. These properties can be determined by the BET method. The BET theory is a rule for the physical adsorption of gas molecule on a solid surface and serves as the basis for an important analytical technique for the measurement of the specific surface area of a material.

The concept of the BET theory is an extension to multilayer adsorption of the Langmuir theory for monolayer molecular adsorption with the following hypotheses:

1. Gas molecules physically adsorb on a solid in layers infinitely;

2. There is no interaction between each adsorption layer; and

3. The Langmuir theory can be applied to each layer.

The resulting BET equation is expressed by the following equation:

$$\frac{1}{v\,[(P_0/P)-1]} = \frac{c-1}{v_m c}\left(\frac{P}{P_0}\right) + \frac{1}{v_m c}$$

P and P_0 are the equilibrium and the saturation pressure of adsorbates at the temperature of adsorption, v is the adsorbed gas quantity (for example, in volume units), and v_m is the monolayer adsorbed gas quantity. c is the BET constant, which is expressed by the following equation:

$$c = \exp\left(\frac{E_1 - E_L}{RT}\right)$$

E_1 is the heat of adsorption for the first layer, and E_L is that for the second and higher layers and is equal to the heat of liquefaction.

The adsorption isotherm can be plotted as a straight line with $1 / v[(P_0 / P) - 1]$ on the y-axis and $\varphi = P / P_0$ on the x-axis. This plot is called a BET plot . The linear relationship of this equation is maintained only in the range of $0.05 < P / P_0 < 0.35$. The value of the slope A and the y-intercept, I, of the line are used to calculate the monolayer adsorbed gas quantity, v_m, and the BET constant, c.

$$v_m = \frac{1}{A + I}$$

$$c = 1 + \frac{A}{I}$$

The BET method is widely used in surface science for the calculation of surface areas of solids by physical adsorption of gas molecules. A total surface area, S_{total} and a specific surface area, S, are evaluated by the following equations:

$$S_{BET,total} = \frac{(v_m N s)}{V}$$

$$S_{BET} = \frac{S_{total}}{a}$$

Where N is avogadro's number, S is adsorption cross section, Vm is molar volume of adsorbent gas, and A is molar weight of adsorbed species.

A large specific surface area is preferable for producing materials with large adsorption capacity. However, the presence of a large internal surface area in a limited volume gives rise to large numbers of small sized pores between adsorption surfaces. The size of these micropores determines the accessibility of adsorbate molecules to the internal adsorption surface. Therefore, this is another important property for characterising adsorptivity, and the isotherm obtained from these adsorption measurements provides information on the surface area, pore volume, and pore size distribution.

Surface polarity corresponds to the affinity with polar substances such as water or alcohols. Polar adsorbents are thus called *hydrophillic*, and aluminosilicates such as zeolites, porous alumina, silica gel or silica-alumina are examples of adsorbents of this type. On the other hand, nonpolar adsorbents are generally *hydrophobic*, and carbonaceous adsorbents, polymers and silicalite are typical nonpolar adsorbents. These adsorbents have more affinity with oil or hydrocarbons than with water.

In this project, specific surface areas, total pore volume, and pore sizedistribution of natural kaolin and samples of kaolin modified by physical and/or chemical treatments were determined by the BET method using N_2 adsorption capacity at 77 K.

2.5.5 Surface charge density (P_{ZC})

The surface charge density is a fundamental description of a mineral surface. At pH values above the P_{ZC}, the surface has a net negative or anionic charge, and the surface

participates in cation attraction, and can adsorb positively charged polar molecules. In contrast, at pH values below the P_{ZC} , the surface has a net positive charge, and participates in anion exchange reactions to adsorb the negatively charged polar molecules.

In this work, the P_{ZC} was determined by titration method. The surface charge (Q) was calculated using the equation:

$$Q = [(C_a - C_b - [H^+] + [OH^-])]/W$$

Where Q is the surface charge (mol/g adsorbent dry weight), C_a is the added acid (mol/L), C_b is the added base (mol/L), W is the dry weight of the adsorbent (g),The point of zero charge (Q = 0) was obtained from plots of Q versus pH

2.6 Modification of kaolin for adsorption of pigments from rice bran oil

2.6.1 Acid activation (Chemical treatment)

As previously described, the kaolin-group minerals are 1:1 layer silicates with structures composed of siloxane and gibbsite-like sheets joined through an apical oxygen. The siloxane sheet consists of silicon tetrahedra in a hexagonal arrangement, whereas the gibbsite-like layer contains aluminum bound to four OH groups and two oxygen atoms in octahedral coordination. The tetrahedral sheet is covered in oxygen atoms (siloxane surface), and the octahedral sheet is covered in hydroxyl groups (aluminol surface). These layers are joined to other layers by hydrogen bonding, and as consequence it is very difficult to modify the surfaces of the kaolin minerals.

Acid-treated clays are commonly used as adsorbents for decolorizing oils. This treatment increases the surface area, porosity, pore volume and acidity of the clay. Surface area is increased by disaggregation of clay particles, elimination of several some mineral impurities and removal of metal cations (Vicente et. al., 1996). The effect of acid activation treatment depends significantly on the type of clay; for example in bentonite the effect was dramatic, but there was little effect on other clays such as kaolinite, attapulgite, etc. The acid activation process sometimes destroys part of the clay layer structure, since it removes iron, aluminum and magnesium from the octahedral sheet. Treatment with cold, dilute acid has little effect on metal ion removal,

but activation with hot, concentration acid results in the removal of metal ions. (Breen, et al. 1997) Acid activation causes little damage to the silicate layer, and consequently the structure in the center of the platelet, at the limit of acid attack, remains intact. The rate of dissolution of the octahedral layer was observed to increase not only with increasing concentration of acid, temperature and contact time, but also with increasing Mg content in the octahedral sheet.

2.6.2 Mechanical activation (Physical treatment)

In addition to acid activation, clays may be modified in a number of other ways. These include mechanochemical activation, modification of the surface through intercalation, adsorption of molecules on the external surfaces, thermal treatment etc.

For mechanical treatment, known quantities of the reactant powders are ground in a planetary ball mill for a fixed period of time. This results in structural alteration and frequently an increase in reactivity of the product. With some materials, chemical reactions are possible during the milling period.

In this process all ball milling is carried out in a vessel or jar, into which the material to be ground is added, along with balls or other suitably shaped grinding elements that are made of the same material as the jar. The grinding process takes place by the interaction between the balls, particles and grinding jar wall, and the technique works equally well on soft, medium-hard and even extremely hard material. In a planetary ball mill, one or more grinding jars can be used, with each occupying a station or *planet* that is mounted on a circular platform called a *sun wheel.*

Mechanical of kaolin surface by mechanical activation.

Mechanical treatments, such as dry grinding, of some minerals, including kaolinite, results in changes in their physicochemical properties (Mendelovici, 2001), and may also result in the formation of new materials with potential industrial applications. Mechanical action causes structural changes in addition to reducing particle sizes to the submicron size and even into nanometer range. This is accompanied by an increase in surface energy, and enhancement of the surface reactivity (Temmujin, et al. 2001) Two types of material are produced, an amorphous aluminosilicate and an agglomerated material. Dry grinding causes kaolin layers to fragment and results in the formation of

spheroidal particles (Gonzalez, et al. 1991). It has been proposed that dry grinding removes hydroxyl groups from kaolinite and results in the formation of a new kaolinite surface.

Many techniques have been used to study the products of dry grinding of kaolins. The most common technique is X-ray diffraction (Gonzalez, et al. 1991), which shows that the kaolinite structure becomes deformed along the c-axis, but is more resilient along b-axis (Schrader, 1970). In that work it was inferred that grinding caused a distortion, but not an actual decomposition, of the kaolinite lattice. The mechanical amorphisation of kaolinite is accompanied by the rupture of O-H, Al-OH, Al-O-Si and Si-O bonds. The product of such amorphisation is a water-containing xerogel with random structure, in which the original hydroxyl groups of kaolinite are converted into coordinated water bound to the kaolinite backbone. This phenomenon is known as prototropy, which involves the interaction of two hydroxyl groups in a two step process to form a water molecule by proton transfer leaving chemically bonded oxygen, as an oxide ion, in the lattice. The reaction may be described as follows (Frost, et al. 2004).

$$OH^- \longrightarrow H^+ + O^{2-}$$

$$H^+ + OH^- \longrightarrow H_2O$$

It is highly likely that point heating at specific sites during grinding is the cause of this reaction, which results in an increase in dehydroxylation with increased grinding time (Rocha, 1999). Proton delocalization at specific hydroxyl sites is required, and this may occur when the mechanochemical treatment of the kaolinite causes heating at the point of contact between two particles. For water to form, protons have to migrate to a second hydroxyl site. If two adjacent hydroxyls are involved in the two step process it will be homogeneous, if, however, non adjacent hydroxyls are involved, such a process would require proton hopping.

From a practical standpoint, solubility characteristics are important in determining the utility of various clays as sources of aluminum and for the production of porous materials. The solubility of kaolinite in acids varies with the nature and concentration of the acid, acid: kaolinite ratio, the temperature and the duration of treatment. Under

similar conditions of acid treatment, kaolinite is more soluble in sulfuric than hydrochloric acid, but after amorphisation by heating or grinding, all or substantially all the alumina of the kaolinite is soluble.

The kaolinite structure consists of two-sheet layers, in which networks of silicon-oxygen tetrahedra [SiO_4] are combined in six-membered rings and connected with [$Al(O,OH)_6$] octahedral on one side of the tetrahedra. The presence of strong hydrogen bonds connecting neighbouring layers protects the aluminum cations against dissolution by acid. Thus, initial modification of the kaolinite structure by treatments, such as mechanochemical activation or thermal treatment, followed by acid activation is a promising approach for the generation of new structures (Boris, et al., 2004).

2.7 Adsorption on clay minerals

2.7.1 Principle of adsorption

The term adsorption is though to have been first used by Kayser in 1881 in order to explain the condensation of gases on surface. Adsorption is described as the enrichment of one or more components in the interfacial layer, i.e. an excess of molecules exists at the adsorbate/adsorbent interface, upon exposure of an absorbing solid to a gas or vapor. It is the selective collection and concentration onto solid surfaces of certain molecules contained in vapours or gas stream. Hence, vapours or gases are referred as adsorbates when adsorbed, and even when present in mixed systems at low concentrations, adsorbates may be captured, often selectivity, and removed the effluent stream using an appropriate adsorbent.

Adsorption can be divided into the two sub-categories: physical adsorption (physisorption) or van der Waals adsorption, and chemical adsorption (chemisorption), depending on whether or not chemical bonds are formed during the adsorption process. Physisorption is applicable to all adsorbate-adsorbent systems, provided the conditions of pressure and temperature are suitable, whereas chemisorption can occur only if the system is capable of making a chemical bond between the adsorbent and adsorbate.

2.7.2 Physical adsorption (Physisorption)

This process is a dynamic one involving an equilibrium state containing adsorbed and desorbed molecules. Chemical bonds are not formed during physical adsorption. The

attraction between the adsorbate and adsorbent exists by the formation of intermolecular electrostatic forces, such as London dispersion forces, or van der Waals forces from induced dipole-dipole interactions, or alternatively it may be dependent on the physical configuration of the adsorbent, such as the porosity of activated carbons. Dispersion forces are the result of rapid fluctuations in the electron density of one adsorbent molecule, including an electrical moment in a second atom. If the adsorbate possesses a permanent dipole, or even a multipole, then additional interactions may occur, as a result of induction of charge distributions in the adsorbent and interactions of these moments with any permanent field in the solid.

The process is a very general one and is analogous to that of condensation. Physisorption occurs to varying extents for all adsorbates, gases and vapours, with all adsorbing solids, and the effect increases with decreasing temperature or increasing pressure. Physical adsorption is based on certain basic considerations, and adsorption on a heterogeneous surface, i.e. a surface on which the sites are different, occurs at the site of highest adsorption potential. The process of physical adsorption into the microporous structure of activated carbon follows the theory of Dubinin.(1966)

The mechanism of adsorption is dependent upon the size of the adsorbate molecule in comparison with the pore width, due to the energetic interaction between the adsorbate and the pore. The process of adsorption is always exothermic, due to the increased order of the adsorbate on the adsorbent surface reducing the entropy according to the equation

$$\Delta G = \Delta H - T\Delta S$$

Thus, according to Le Chatelier's principle, the amount adsorbed should increase with decreasing temperature, since a reduction in the thermal energy supplied to the process favours the exothermic process of adsorption and increases the equilibrium uptake. It has been proposed by Lamond and Marsh(1964) from results for physical adsorption of nitrogen on both polar and non-polar surfaces that physical adsorption is independent of the surface chemistry of the adsorbent.

2.7.3 Chemical adsorption (Chemisorption)

Chemisorption involves the transfer of electrons between the adsorbent and the adsorbate with the formation of chemical bonds. Adhesion of the adsorbate molecules is thus the consequence of chemical reaction between the two species. Chemical adsorption is far less common than physical adsorption, and because of the formation of chemical bonds, regeneration of the adsorbent for subsequent reuse is sometimes difficult or impossible.

Due to the fact that chemical bonds are formed during the adsorption process, desorption of the adsorbed phase may yield products which are chemically different from the original adsorbate. For example oxygen may chemically bond to the surface of carbon, which upon desorption may evolve CO and CO_2 as products.

Table 2.5 The characteristic of physical and chemical adsorption (Soure: Atkins, 1994)

Characteristics	**Physical Adsorption**	**Chemical Adsorption**
Heat of adsorption (kJ/mol)	20-40	> 80
Rate of adsorption (at 273 K)	fast	slow
Temperature dependence of uptake (with increasing T)	decrease	increase
Desorption	easy-by reduced pressure or increase temperature	difficult-high temperature required to break bonds
Desorbed Species	adsorbate unchanged	may be different to original adsorptive
Specificity	non-specific	very specific
Monolayer Coverage	mono or multilayer condition dependent	monolayer

2.7.4 Force of adsorption

The forces responsible for adsorption reactions include physical force, hydrogen bond, hydrophobic bond, electrostatic bond, coordination reactions, and ligand exchange.

1. Physical forces

The most important physical force is the van der Waals force, which results from short-range dipole-dipole interactions and do not involved a significant change in the electronic orbital patterns of the species involved. Its role is of importance only at close distances, since this type of force decreases rapidly with distance.

2. Hydrogen bond

The bond by which a hydrogen atom acts as the connecting linkage is called a hydrogen bond. It's weaker than an ionic bond or covalent bond but stronger than van der Waals. Water, which is a polar molecule, may become adsorbed at a clay surface through its linkage with a hydrogen bond.

3. Hydrophobic bond

Hydrophobic bonds are associated with the adsorption of nonpolar compounds such as hydrocarbon. These compete with water molecules for adsorption sites and result in adsorbed water being exchanged or expelled by the substance.

4. Electrostatic bond

Another type of force in adsorption is electrostatic attraction of substances, which is the result of an electrical charge on the colloid surface. This is the reason for (1) adsorption of water (2) adsorption of cations, which leads to cation exchange reactions, and (3) adsorption of organic compounds. This may develop into complex reactions. Exchange of an organic ligand on a cation is called ligand exchange.

5. Coordination reaction

This reaction involves the formation of a covalent bond, which occurs when a ligand donates an electron pair to a metal ion, usually a transition metal, for example, the adsorption of Pb^{2+} onto the organoclay. The compound formed is called a coordination compound, complex compound, or an organometallic complex. When it involves a reaction between an organic ligand and a metal ion only, the distinction between adsorbate and adsorbents may become obscured.

6. Ligand exchange

The ligan exchange process have the significantly greater selectivity and adsorption capacity than ion exchange. It involves the replacement of a ligand by an adsorbate molecule, which has a stronger chelating capacity than the ligand. The replacement is not limited to expulsion by cations, and the adsorbed organic ligand can also be replaced by other organic compounds.

2.7.5 Adsorption isotherms

Adsorption was defined earlier as the concentration of molecules at colloidal surfaces. The curve relating the concentration of adsorbed materials at a fixed temperature is called the adsorption isotherm. The mass adsorbed is typically plotted on the y-axis and that in the fluid on the x-axis. The shape of the curve is significant and factors heavily into design. Favorable isotherms permit higher solid loading at lower solution concentration. These tend to start out steep and level out. Isotherms which start out flat are unfavorable, since they only work well at high concentrations of solute.

Four major types of equations are used to describe adsorption isotherms: the Freundlich equation, the Langmuir equation, the BET (Brunaner, Emmett, and Teller) equation, and the Gibbs equation.

1. Freundlich equation

The adsorption isotherm for many dilute solutions was formulated by Freundlich (1926) as:

$$x/m = K_F C^{1/n} \qquad (1)$$

where x is mass of material adsorbed, m is mass of adsorbens, C is concentration of the equilibrium solution, K_F, and n are constants

The value of 1/n is usually between 0.2 and 0.7 (Kruyt, 1947), but for many pesticides at dilute concentrations 1/n = 60 (R.A. Leonard, personal communication). The equation has no theoretical foundation and is empirical. The curve according to Equation (1) is usually parabolic and exhibits the following characteristic features: (1) there is no single point indicating that the process is completed; and (2) there is no region of discontinuity. By taking the logarithm, Equation (1) becomes

$$\log x/m = \log K_F + 1/n \log C$$

The log equation gives a linear plot, in which Log K_F is the intercept, and 1/n represents the slope of the curve, or the regression coefficient.

Another version of the Freundlich equation is

$$S = k_d C^n \qquad (2)$$

Where S is mass of solute retained per unit mass of adsorbent (mg/kg), k_d is distribution coefficient, C is solute concentration (mg/kg), and n is dimensionless parameter, typically 1.

The distribution coefficient describes the partitioning of the solute between solid and liquid phases, and is considered analogous to the equilibrium constant in the mass action law equation. With minerals, strongly adsorbed heavy metals, such as Cu, Hg, Pb, and V exhibit high k_d values. The k_d value is also affected by pH and the cation exchange capacity (CEC). Minerals with high pH and CEC values adsorb larger amounts of the heavy metals.

A third version of the Freundlich equation is called the Van Bemmelen-Freundlich equation:

$$\Gamma = Ac^{\beta} \qquad (3)$$

Where Γ is the amount adsorbe, c is the concentration of trace metal cations in the aqueous solution containing the adsorbent, A and ß are empirical parameters with $0 < ß < 1.0$. Therefore, ß is positive, but always lower than 1

This equation is used to describe adsorption of trace metals at constant temperature by clay minerals and sesquioxides in soils. It is an equation without chemical foundation, but it has the ability to describe adsorption data obtained at constant temperature (Sposito,1980). The equation has often been associated with adsorption by heterogeneous surfaces.

In the present work, the Freundlich equation was used in the following form:

$$X = K_F Ce^{1/n}$$

$$Log\, X = (1/n) \log Ce + \log K_F$$

$$X = \frac{(Co\text{-}Ce)V}{1000\, m}$$

Where Ce is equilibrium concentration of Chlorophyll-a (mg/kg), X *is* the amount of Chlorophyll adsorbed per gram of GKS 2 (mg/g), K_F and 1/n are Frundlich constant (parameter), V is mass of rice bran oil (g), m is mass of GKS 2 (g)

2. Langmuir Equation

Another method for describing adsorption was given by Langmuir (1916-1918):

$$\frac{X}{m} = \frac{k_1 C}{1+k_2 C} \qquad (4)$$

Where x is mass adsorbed, m is mass of adsorbent, k_1,and k_2 are constants, C is concentration of equilibrium solution

The Langmuir equation differs from that of Freundlich in that at very high concentration, k_2C in Equation (4) is sufficiently large that the factor 1 can be neglected, so that the formula becomes simply

$$x/m = k_1/k_2$$

Thus x/m is constant at high concentration, C, the surface of the adsorbent becomes saturated, and adsorption reaches a maximum.

In the present work, the Langmuir equation is as follows

$$\frac{Ce}{X} = \frac{1}{K_L X_m} + \frac{1}{X_m} Ce$$

$$X = \frac{(Co-Ce)V}{1000\, m}$$

Where Ce is equilibrium concentration of Chlorophyll-a (mg/kg), X is the amount of Chlorophyll adsorbed per gram of GKS 2 (mg/g), K_L and X_m are Langmuir constant (parameter), V is mass of rice bran oil(g), and m is mass of GKS 2 (g)

3. Brunauer, Emmett, and Teller Equation

The BET equation was developed by these authors in 1938 for the adsorption of multilayers of nonpolar gases. The equation at low pressure is as follows:

$$\frac{P}{V(Po-P)} = \frac{1}{VmC} + \frac{C-1}{VmC}\frac{P}{Po} \qquad (5)$$

Where P is equilibrium vapor pressure , P_o is saturation vapor pressure , V is volume of gas adsorbed, V_m is volume of gas adsorbed when solid is covered with monolayer, and C is constant related to heat of adsorption

The BET equation is an extension of the Langmuir equation for application to multilayer adsorption. It is assumed that the first layer is attracted firmly to the surface, perhaps by van der Waals forces. The second and subsequent layers are held by weaker forces. As P/P_o increases, the layers of gas are built up in an unrestricted way. The number of layers becomes infinite when P/P_o is unity. If $P/[V(P_o - P)]$ is plotted against P/P_o (as the abscissa), a linear relationship should be obtained. The slope is characterized by the factor $(C - 1)/V_mC$, and the intercept is at $1/V_mC$.

4. Gibbs Equation

The Gibbs equation describes adsorption processes in relation to surface tension.

$$\Gamma = -\frac{x}{RT}\left(\frac{d\sigma}{dx}\right)_T$$

Where Γ is surface concentration of adsorbed material, x is bulk concentration expressed in molar fraction, σ is surface tension in dyne/cm, R is gas constant, and T is absolute temperature. If $d\sigma/dx$ is negative, the solute would be adsorbed on the surface of the adsorbents, in contrast the solute would be more concentrated in the bulk solution than in the interface region if it is positive.

2.8 Rice bran oil

2.8.1 Rice bran and rice bran oil

Rice (*Oryzae Sativa* L.) is the principle staple food for about half of the World's population. It is grown in more than one hundred countries, under a variety of climatic conditions (Wadsworth, 1992). When harvested from the field, rice is in the form of paddy rice (or rough rice), where the kernel is fully enveloped by rice hull. The structure of the rice kernel is illustrated in Figure 2.24.

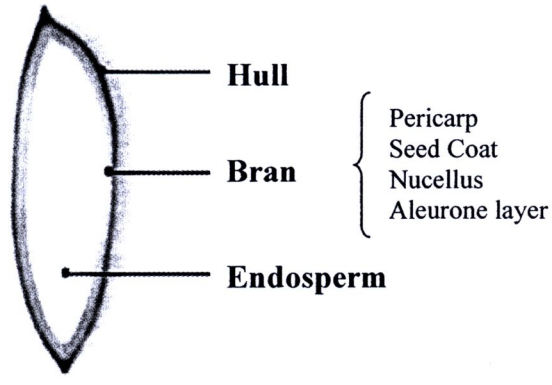

Figure 2.24 The structure of the rice kernel

After being dried, the hull is removed in the first stage of milling, yielding the brown rice. In the second stage of milling, the outer brown layer is removed to produce the white rice. The outer brown layer is called the rice bran. Rice bran is primarily composed of pericarp, aleurone, and subaleurone layers of the kernel, and typically includes the embryo or germ and a small amount of starchy endosperm (Tahira, et al., 2007). Rice bran oil is a byproduct of rice milling and has been used for centuries in many Southeast Asia countries. Typically, rice bran oil comprises about 20% saturated fatty acid and an even balance of monounsaturated and polyunsaturated fatty acids (40:40); it contains relatively large amounts of unsaponifiable components (3-5%). In recent years, the oil has gained world wide attention due to the presence of several components considered to have health benefits, such as a unique complex of naturally occurring antioxidant components, tocopherols, tocotrienols, oryzanol, phytosterols and phytostenols (Lloyd, et al., 2000; Diack and Saska, 1994). Vitamin E is a generic term for a group of four tocopherols and four tocotrienols. A number of studies have reported that vitamin E functions as a chain-breaking antioxidant that prevents the propagation of free radical reactions (Brigeliusflohe and Trabet, 1999; Becker, et al., 2004; Huang, et

al., 2002). Oryzanol is a mixture of esters of ferulic acid with sterols and triterpene alcohols with similar antioxidant properties to vitamin E (Shin, et al., 1997), and has been linked to inhibition of platelet aggregation (Cicero and Gaddi, 2001). Furthermore, phytosterols and phytostanols have received much attention in the last five years because of their cholesterol-lowering properties, although early phytosterol-enriched products contained free phytosterols and relatively large dosages were required to significantly lower serum cholesterol (Moreau, et al., 2002)

The lipid composition of crude rice bran oil, and the physical and chemical characteristics and fatty acid composition of refined rice bran oil are presented in Tables 2.4 and 2.5, respectively.

Table 2.6 Lipid composition of crude rice bran oil
(Source : Sayre and Saunders, 1990 ; Orthoefer, 1996)

Saponifiable lipids (90 – 96 % w)		Unsaponifiable lipids (4.2 % w)	
Neutral lipids	88-89	Phytosterols	43
Triglycerides	83-86	Sterolesters	10
Diglycerides	3-4	Triterpene alcohols	28
Monoglycerides	6-7	Hydrocarbons	18
Free fatty acids	2-4	Tocopherols	3
Waxes	3-4		
Glycolipids	6-7		
Phospholipids	4-5		

Table 2.7 Physical – chemical characteristics of refined rice bran oil (Source: Sayre and Saunders, 1990; Orthoefer, 1996; Firestone1999; Krishna, 2000)

Parameter	Typical	Range
Refractive index (20° C)	1.470	1.470 -1.474
Specific gravity (20° C)	0.916	0.916 - 0.922
Iodine value	95	90-110
Free fatty acid value (as % oleic)	0.05	0.05-0.12
Saponification value	193	180-195
Smoke point (°C)	213	-
Colour Lovibond (5.25 inch)	2.5 R,27 Y	2.5-3.5 R, 25-35 Y
Fatty acid composition (% w)		
14:0	0.4	0.2-0.7
16:0	19.8	12-28
16:1	0.2	0.1-0.5
18:0	1.9	2-4
18:1	42.3	35-50
18:2	31.9	29-45
18:3	1.2	0.5-1.8
20:0	0.9	0.5-1.2
20:1	0.5	0.3-1.0
22:0	0.3	0.1-1.0
Others	0.6	1.0 max

THE NATIONAL RESEARCH COUNCIL OF THAILAND RESEARCH LIBRARY

2.8.2 Rice bran oil extraction process

Rice bran oil contains 2-4% free fatty acids at the time of milling. If not immediately extracted, the lipids in freshly milled rice bran undergo hydrolysis due to the presence of a potent lipase. To obtain good quality rice bran oil, it is important to stabilize the bran quickly prior to extraction. The methods of stabilizing rice bran include dry heat, wet heat, and extrusion. For example, if the bran is subjected to a short-term high temperature heat treatment, immediately after milling, lipase activity is destroyed and

stabilized bran is produced. Heat stabilization at 125-135°C for 1-3 s at 11-15% moisture causes no adverse effect on bran nutritional quality.

Hexane is generally used for counter-current extraction of the stabilized bran material in batch or continuous operation. The pre-treated bran flakes/pellets are placed in an extractor, hexane is pumped in, and allowed to percolate through the bran to extract oil. Though, waxes are soluble in hot hexane, an extraction temperature between 30-50°C gives optimized oil extraction without excessive wax removal. The extracted oil and hexane micelles are transferred to a solvent recovery unit for production of crude rice bran oil. The cake is treated separately with stripping steam in a desolventiser/toaster to remove residual solvent. The lipid composition of good quality, crude rice bran oil is presented in Table 2.6. The crude oil is usually dark greenish-brown, depending upon extraction method, bran condition, composition and pigments.

2.8.3 Rice bran oil refining

The composition of the crude oil has a major influence on the refining method and conditions used. Rice bran oil is usually difficult to refine due to high free fatty acid (FFA) levels, waxes, bran fines and pigments. In general, traditional refining of rice bran oil involves dewaxing, degumming, neutralization, bleaching to improve color and steam deodorization. The Thai Edible Oil Co.,Ltd. (Thailand) has reviewed the methods of refining rice bran oil in order to obtain high quality refined rice bran oil. The refining process begins by degumming and neutralization. Degumming with food-grade phosphoric acid is carried out to precipitate gums, metals and other undesirable components from the oil. Depending upon the FFA content, the degummed or acid pretreated oil is then neutralized with 16-30 Baume caustic with 20-40% excess. Soap-stock separation temperatures in the region of 55-70°C are reported to work well. The refined oil is washed with water to remove traces of soaps and dried, prior to bleaching for removal of color pigments and other undesirable components with activated clay. After decreasing color, the oil is forwarded to the crystallization process before filtering the wax through a filter press machine. The next process is to remove odor by using a high-pressure steam deodorizer at a temperature of 230-240°C. The heating medium used in this process is high pressure steam. The result is high quality rice bran oil. A description of the rice bran oil process used by the Thai Edible Oil Co., Ltd. is presented in Figure 2.25.

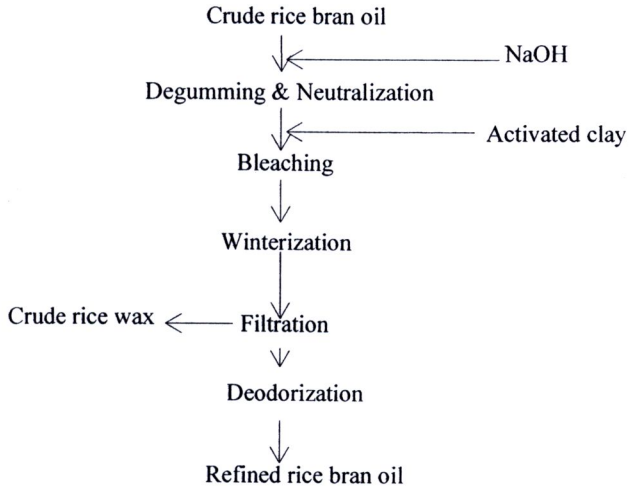

Figure 2.25 Diagrammatic presentation of rice bran oil processing as used by the Thai Edible Oil Co., Ltd.

2.8.4 Chlorophyll

Chlorophyll is the green pigment molecule in plant cells that carries out the bulk of energy fixation in the process of photosynthesis. Chlorophyll itself is actually not a single molecule but a family of related molecules, designated chlorophyll a, b, c, and d. Chlorophyll-a is the molecule found in all plant cells, and therefore its concentration is what is reported during chlorophyll analysis. Chlorophyll-d is found only in marine red algae, and chlorophyll-b and -c are common in fresh water algae. The molecular structure of chlorophyll-a and –b consists of a ring-like structure called a porphyrin and a long organic phytol, tail. In the center of the porphyrin ring is magnesium molecule (Figure 2.26). Chlorophyll-c lacks the phytol chain.

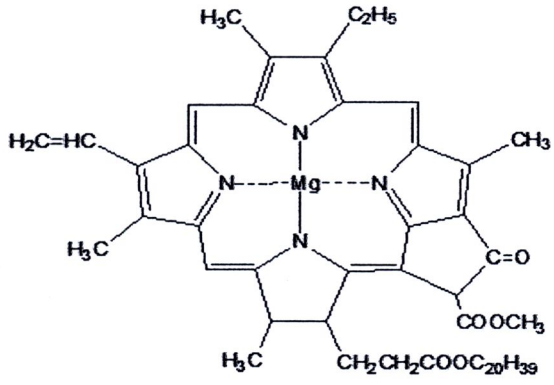

Chlorophyll a

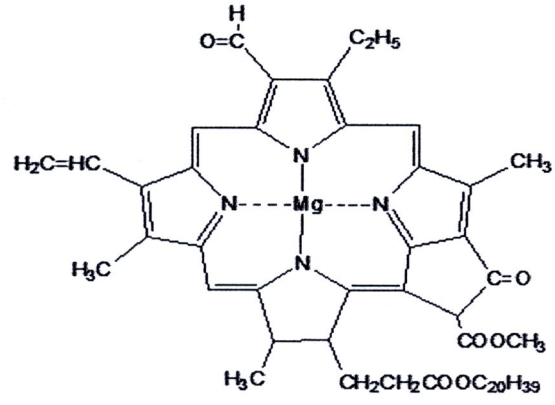

Chlorophyll b

Figure 2.26 The chlorophyll-a / b molecule

Chlorophyll-a ($C_{55}H_{72}MgN_4O_5$) is the one of colored compounds in oil that must be removed in the bleaching process. It imparts a greenish color to the crude oil, but if this oil is then processed by conventional refining techniques the chlorophyll is converted to the pigment pheophytin, which gives oil a dark, dull brown tinge, and contributes to an off-flavor. It may also promote oxidation of the oil, and reduce its storage stability (Levente, 2005).

The intense green color of chlorophyll is due to its strong absorbance in the red and blue regions of the spectrum (Figure 2.27). Because of this absorbance, the light it reflects and transmits appears green.

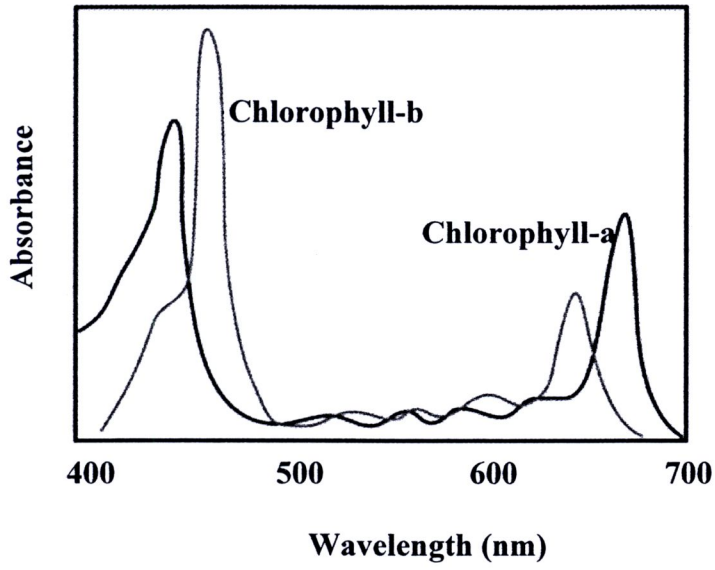

Figure 2.27 The UV/VIS absorption spectrum of chlorophyll-a / b

Due to its green color, chlorophyll has many uses as dyes and pigments. It is used in coloring soaps, oils, waxes and confectionary. Commercial pigments with structures similar to that of chlorophyll have been produced in a range of colors. Some of these have slightly modified porphyrins, such as having hydrogen atoms replaced with chlorine atoms. Others have different metal ions. For example, one bright blue pigment has a copper (II) ion at the center of the porphyrin and is used primarily in coloring fabrics. (Berezin, et al.,2003)

2.8.5 Analysis of oil

Peroxide value and acid value determination

The peroxide value (PV) and acid value (AV) are usually considered to be the main parameters reflecting the quality of vegetable oil, degree of refining, as well as the quality change during storage. The peroxide value of oil is used as an indicator of oxidative rancidity, whereas the acid value is used as an indicator of the triglyceride oxidation. Both values are affected by the age of raw materials as well as oxidation of oil during processing and storage.

The peroxide value is defined as the amount of peroxide oxygen per kilogram of fat or oil. Traditionally this was expressed in units of milliequivalents, although if using SI

units then the appropriate unit is millimole per kilogram (1 millimole = 2 milliequivalents). Note also that the unit of milliequivalent has been commonly abbreviated as mequiv or even as meq.

The acid value (AV) is defined as the number of milligrams of potassium hydroxide necessary to neutralize the free acids contained in 1 gram of sample. The majority of national and international standards for AV determination in vegetable oils are based on the acid-base titration techniques in non-aqueous solvents.

Oils are oxidized at the sites of unsaturated bonds in fatty acid chains. This results in the production of a variety of compounds, including free radicals and hydroperoxides, as well as epoxides, aldehydes and ketones. At the onset of oxidation, the peroxide value increases but then falls in the later stages of oxidation as samples are oxidized to aldehydes and ketones. For peroxide value determination, oil is mixed with a solvent, and potassium iodide is added to the solution of the oil. Peroxides and other oxidizing material in the oil react with the iodide to liberate iodine. The reaction proceeds for a specified time and is then stopped by diluting the reaction mixture.

$$2I^- + H_2O + ROOH \longrightarrow ROH + 2OH^- + I_2$$

The amount of iodine liberated under the specific condition of the test is measured by titration with sodium thiosulphate. Note that the base produced in this reaction is taken up by the excess of acid present.

$$2S_2O_3^{2-} + I_2 \longrightarrow S_4O_6^{2-} + 2I^-$$

Acidic conditions (excess acetic acid) prevents formation of hypoiodite (analogous to hypocholite), which would interfere with the reaction. The indicator used in this reaction is a starch solution where amylose forms a blue to black solution with iodine and becomes colorless when the iodine is titrated. A precaution that should be observed is to add the starch indicator solution only near the end point (i.e. when fading of the yellowish iodine color occurs), because at high iodine concentration starch is decomposed to products whose indicator properties are not entirely reversible.

2.9 Literature review

2.9.1 Acid activated clays

Kheok and Lim (1982) studied the mechanism of bleaching of palm oil by a non-swelling montmorillonite clay activated by H_2SO_4 at concentrations of 10-40 %. The study showed that an initial increase in bleaching ability by clay activated by an increasing addition of H_2SO_4 was due to acid leaching of organic matter and impurities in the clay. The consequence of acid leaching also removed Al^{3+}, causing charge deficiency in the clay lattice and, hence, promoting the adsorption properties of the clay. A drop in bleaching efficiency at higher additions of H_2SO_4 was observed. This was due to excessive acid leaching of Al^{3+}, causing collapse of the clay lattice structure.

Makaya, et al. (1993) studied chlorophyll adsorption by alumina-pillared acid activated clays. Acid activated clays were pillared with alumina to give semi-crystalline expanded materials with surface acidities, pore volumes and average pore diameters generally higher than those of the corresponding pillared materials derived form a clay matrix not previously acid-activated. They reported that the chlorophyll adsorption capacity of the pillared acid-activated materials was significantly greater than that of pillared, non-activated clays. Procedures used in the preparation of these pillared acid-activated clays (i.e., temperature of pillaring, method of drying and calcination temperature) had a significant influence on chlorophyll adsorption capacity, because they affect both the physical and the chemical properties of the final pillared material. This variation provides a useful means for relating the various properties of the pillared materials to the chlorophyll adsorption capacity. As a result, a correlation was demonstrated between adsorption capacity and a combination of pore volume and number of strongly acidic sites (of strength pKa < - 1.5) present in the pillared material. Optimal adsorbents were obtained from freeze-dried samples prepared by exchange at 20°C and calcined in air at 500°C.

Makaya, et al. (1994) also studied the mechanism of chlorophyll adsorption on acid activated montmorillonite. They reported that the influence of the exchangeable cation on the adsorption process decreased with increasing levels of acid activation, suggesting a possible existence of acid sites not associated with the cation. The nature of the acidity

of the adsorbent (clay) changed following adsorption of chlorophyll, which is believed to adsorb as a protonated species.

Kumar, et al. (1995) studied the evolution of surface acidity and porosity in montmorillonite on treating with H_2SO_4. Maximum surface acidity was observed when the clay was treated with 4 N acid. Acid strength distribution as measured by Benedi's technique of non-aqueous titration shows acidity range mainly between H_o +4.6 and +3.3. N_2 adsorption-desorption hysteresis data indicated the transformation of pores from slit-shaped to spheroidal or ink bottle type as the acid concentration was increased from 1 to 8 N. These observations were explained in terms of structural modifications of clay on treatment with acid.

Falaras, et al. (2000) investigated the bleaching of cottonseed oil by alumina-pillared (Al-pillared) acid activated montmorillonite. Acid activation of Ca-rich montmorillonite following treatment with 1, 4, and 8 eq/L H_2SO_4, as well as subsequent pillaring with alumina, produced new materials. They found that these materials have bleaching properties dependent upon the extent of activation of the clay prior to pillaring. The pillared acid activated montmorillonites possessed higher bleaching efficency compared to pillared products of untreated clay. Mild activation of the clay matrix, pillaring with the Keggin ion $[Al_{13}O_4(OH)_{24}(H_2O)_{12}]^{7+}$, and calcination temperature of 500°C produced materials with the best fractional degree of bleaching. Optimization of the bleaching process was achieved via a judicious utilization of intermediate surface area, relatively high acidity, and enhanced pore volume.

Christidis and Kosiari (2003) studied the mechanism of decolorization of crude maize and sunflower oils, by means of adsorption of ß-carotene, by a low-grade bentonite, containing mixed-layered illite-smectite. The study found that decolorization depends on temperature, and the time required for equilibrium decreased with increasing temperature. Study of the kinetics of adsorption showed that decolorization of maize oil is a first-order process, described by a single mechanism with intermediate activation energy (19.0 kJ / mol). Adsorption isotherms for decolorization of maize oil follow the Freundlich equation, indicating the existence of heterogeneous adsorption sites on the solid surface. The heterogeneity was attributed both to different active centers on the

smectite surface (Bronsted and Lewis centers) and to different phases present in bentonite, such as illitic layers and clinoptilolite, which also have active centers on their surfaces.

Temuujin, et al. (2004) studied the characteristics of acid leached montmorillonite-containing clay from Mongolia by XRD, DTA-TG, FTIR and N_2 adsorption technique. Samples were treated with 2 M HCl (Liquor: Material = 1:25) at 80°C for 1 h, 2, h, 6 h, and 12 h. The study found that leaching caused the surface area of the clay to increase 3-fold to 93.9 m^2/g, reflecting the formation in the porous silica product of 3-5 nm micropores and 6-10 nm mesopores; the latter resulted from a delaminated card-house structure rather than from the condensation of the micropores. Differences between the surface areas of these leached samples and those reported for other montmorillonite clays reflect the mineralogical composition of the clay, particularly the presence of non-clay constituents associated with the surface.

Foletto, et al. (2006) studied the structural properties and bleaching efficiency of acid-treated bentonites. Two natural bentonites were treated with 4 and 8 N HCl for 2 h. Clarification efficiency was strongly dependent on the acid concentration and natural clay mineral compositions used to activate the bentonite for the clarification process.

Temuujin, et al. (2006) studied nanoporous materials prepared from montmorillonite clay that was purified by leaching with 0.5 - 2 M H_2SO_4 at 80°C for 0.5-4 h. They reported that acid leaching caused partial amorphization of the clay with depletion of MgO, Al_2O_3, CaO, and Fe_2O_3 components mostly from interlayer and octahedral sites. This increased the specific surface area by more than 3 times, i.e. from 49.1 to 157 m^2/g. The pore-size distribution curve calculated from the adsorption isotherms of the leached montmorillonite show that most of the pores are in the mesoporous region with diameters of 3-4 nm. The highest acidity was achieved by treating the clay with 0.5 M H_2SO_4 for 4 h. This material was found to be appropriate for bleaching of mare's milk oil, in which ß-carotene is the main pigment.

Ugarla and Kuba (2007) studied the effect of adsorption time, temperature and solid: liquid ratio on the capacity of sepiolite to adsorb coloured material from olive oil. It was

found that thermally acid activated sepiolite (AAS) was more efficient than thermally activated sepiolite (AS). Adsorption equilibria of carotene and FFA were described by the Frundlich models, and a higher adsorption coefficient (K) was observed for AAS ($K_{carotene}$ = 2.73x10^{-3} mg/g, K_{FFA} = 0.98 mg/g) compared to AS ($K_{carotene}$ = 2.63x10^{-7} mg/g, K_{FFA} = 0.21 mg/g). Moreover, the rate constants obtained for carotene and colour by using AAS (k_{colour} = 0.0241 min^{-1} ,$k_{carotene}$ = 0.0217 min^{-1}) were higher than that of AS (k_{colour} = 0.01 min^{-1}, $k_{carotene}$ = 0.0165 min^{-1}) 42.3 to 1.60 mg/kg under optimum condition of 100°C bleaching temperature and 1.5% sepiolite dosage. It was shown that the reaction is entropy driven and physical in nature, suggesting that ß-carotene molecules adsorb both directly on the meso-external surface of acid activated sepiolite and also penetrate intra-crystalline channels and tunnels.

Sabah (2007) studied the adsorption characteristics of acid activated sepiolite (AAS) for the removal of chlorophyll-a from rapeseed oil. The adsorption equilibrium was found to follow the Langmuir isotherm model with a maximum adsorption capacity of 0.36 mg/g on AAS. Thus, AAS is an effective adsorbent for the removal of chlorophyll-a molecule, which is believed to adsorb as protonated species onto Si-OH groups at the edge in the tetrahedral sheet of sepiolite. These findings reveal that chlorophyll-a molecules not only adsorb onto the external surface of AAS but depending on the pore size can replace the Mg^{2+} ions released from the octahedral sheet.

Huang, et al. (2007) studied the pore size distribution and specific surface area of attapulgite for uptake of pigments from oil. The Frundlich isotherm analysis was used to evaluate the sorption capacity of three attapulgite samples. Two samples had more micropores smaller than 15 Å, but only one had some larger pores in the 100-700 Å range. There were also differences in the pore size distributions, which was the main factor determining the adsorption capacity. They found that the more pores with a distribution range of 8-32 Å (i.e., close to the diameter of the pigments), the more pigments were removed.

Noyan, et al. (2007) studied the bleaching power of acid activated bentonite towards soybean oil. The natural bentonite was activated with H_2SO_4 by a dry method at 97°C for 6 h. Its crystallinity was examined by XRD before and after activation, and the

specific surface area (S), specific micro-mesopore volume (V), mesopore size distribution (PSD), and surface acidity (n_m) were also determined. S, V, n_m and bleaching power (BP) all increased after activation with various acid concentrations up to 40% H_2SO_4 without any significant change in the crystal structure of the smectite. The BP was controlled more by the PSD than the other adsorption properties of the clay. The optimum parameters for activation are H_2SO_4 50-60%, S 250-230 m^2/g, V 0.46 – 0.47 cm^3/g, n_m $9.0x10^{-4}$ - $8.4x10^{-4}$ mol/g, and PSD distributed mainly between 1.4 and 6.0 nm.

2.9.2 Mechanochemically-treated clays

Sugiyama, et al. (1994) studied the structure of ground kaolinite and pyrophyllite by the radial distribution function (RDF) from X-ray diffraction data. There was a decrease in the oxygen coordination number and the corresponding interatomic distance around aluminum with increasing dry grinding time. The SiO_4 tetrahedra remained unchanged in both ground kaolinite and pyrophyllite samples.

Okada, et al. (1998) studied the preparation of microporous silica by calcining kaolinite at 600°C for 24 h and then treating the metakaolinite product with 20% H_2SO_4 at 90°C for 0.5 – 5 h. The Al_2O_3 content decreased dramatically after leaching with 20% H_2SO_4, whereas the SiO_2 content reached > 90% after 1.5 h leaching. Specific surface areas of products were around 340 m^2/g, micropore volumes around 0.18 ml/g and average pore diameter 0.6 nm. The micropores are suggested to occur in the interlayer regions between the SiO_4 tetrahedron layers.

Temuujin, et al. (2001) also studied the preparation of porous silica from mechanically activated kaolinite. This mesoporous material was prepared by leaching Al_2O_3 from amorphized kaolinite with 20% H_2SO_4 at 90°C for 30, 60, 120, and 240 min. Amorphizied kaolinite was prepared by dry grinding in a planetary ball mill for 1 h. The porous material with different properties, was studied by XRD, XRF, FTIR and BET, and it was found that SSA was 312 - 284 m^2/g, and the PSD showed a unimodal pore size distribution with an average of about 3.8 nm. The total pore volume of the silica product was 0.28 - 0.312 m^2/g. NMR measurements suggested that grinding kaolinite affects the octahedral more than the tetrahedron layers. Spectra of the leached products showed peaks at –102 and -11 ppm, assigned to the silanol group and the 3-D silica

framework, respectively. By the Horvath-Kawazoe method, micropore size distribution showed a maximum at 0.9 nm with 30 min leaching time, but the number of micropores decreased with longer leaching times due to a condensation reaction.

Frost, et al. (2002) studied the modification of kaolinite surfaces through mechano-chemical treatment by IR spectroscopy. Kaolinite samples were ground in a planetary mill for 0, 0.5, 1, 2, 3, 4, 5, 6, or 10 h. It was found that the intensity of hydroxyl-stretching bands decreased and there was a concomitant increase in intensity of bands attributable to water hydroxyl-stretching vibrations. Thus, infrared spectroscopy showed that the kaolinite surface was modified by removal of hydroxyl groups and their replacement with adsorbed water.

Temuujin, et al. (2002) studied the effect of dry grinding followed by selective leaching on the preparation of porous material from talc ($Mg_3Si_4O_{10}(OH)_2$), a 2:1 layer silicate. The results showed that grinding exerts a significant effect on the porous properties; the S_{BET} value increased 7-fold to 76.8 m^2/g after grinding and 18-fold to 186 m^2/g after grinding followed by leaching. The pore volume in the ground and leached product (0.53 ml/g) suggested the presence of significant numbers of mesopores and macropores.

Temuujin, et al. (2003) studied the effects on pyrophyllite of grinding for 3-18 h followed by leaching with 4 M HCl at 80°C for 2 h. It was found that the surface area increased with the shorter grinding times, but decreased with longer times.

Kameda, et al. (2004) studied the mechanochemical treatment of kaolinite by grinding for periods in the range 60 - 600 min. XRD showed that the main effect was delamination of layers. IR reflectance spectra showed that kaolinite hydroxyl groups were replaced by surface adsorbed water. H_2 generation through reaction between surface water molecules and mechanically generated radicals occurred by the rupture of Si-O or Al–O–Si bonds. The surface area increased in the early stages of treatment, but was constant for times > 240 min.

Sanchez-Soto, et al. (2000) studied the effect of dry grinding on the structural changes of kaolinite powders. Two kaolinite samples from Georgia, one well-crystallized (KGa-

1) and one poorly-crystallized (KGa-2) were ground by ball-milling. It was found that grinding effected strong structural alterations, mainly along the c axis. These resulted in disorder and total degradation of the crystal structure of kaolinite, and the formation of amorphous material. The surface area increased with grinding time, mainly in KGa-2, and the particle size decreased. These particles became more agglomerated with prolonged grinding, and scanning electron microscopy and particle-size distribution analysis indicated that the surface area decreased after 30 min. There was thus a limit to particle-size reduction that could be achieved with increased grinding times.

Mako, et al. (2006) studied modifications of meohanochemically activated kaolinites by selective leaching. Low-and high-defect kaolinites were ground for ¼, 1, and 2 h using a planetary mill, then leached with 20% H_2SO_4 for 2 h at 90°C. The specific surface area of the leached samples from the partially or the completely amorphized materials were greater than those from the thermally amorphized sample. Acid leaching resulted in a greater total pore volume for the partially amorphized materials than for the totally amorphized mineral under similar conditions.

Minjigmaa, et al. (2007) studied the solubility of fluorapatite.after milling for 60 and 90 min in a vibration mill. Milling decreased the intensity of both quartz and apatite components, but neither full amorphisation nor the appearance of new phases was observed. The solubility of fluoropatite in citric acid improved due to the mechanical treatment; 45% of the total P_2O_5 was converted to a soluble form and the solubility increase from 6% to 17%. However, increasing the milling time from 60 to 90 min decreased the solubility. The specific surface area increased with 60 min milling, but then slightly decreased with 90, suggesting some agglomeration of the milled powders.

Meenakshi, et al. (2008) studied the effect of mechanical treatment of kaolinite on its capacity for fluoride adsorption. When kaolinite was ground with an oscillatory disc mill for 10 min, the surface area increased from 15.11 m^2/g to 32.43 m^2/g. and sorption of fluoride was observed over a wide pH range of 3-11. The adsorption process was fitted by both Freundlich and Langmuir isotherms. Thermodynamic studies revealed that the sorption of fluoride on mechanically activated kaolinite is endothermic and a spontaneous process. The kinetic studies showed that the sorption process followed pseudo-first-order kinetics and intraparticle diffusion models. FTIR spectra revealed

that fluoride removal also followed an ion exchange mechanism in addition to adsorption.

2.9.3 Kaolinite adsorption

O'Day, et al. (1994) studied the adsorption of Co(II) complexes on kaolinite at ambient temperature and pressure in contact with an aqueous solution. The data from analysis of extended X-ray adsorption fine structure (EXAFS) show that, at the lowest amounts of Co uptake on kaolinite (0.20-0.32 $\mu mol/m^2$), the Co is surrounded by ~ 6 O atoms at 2.04 – 2.08 Å and a small number of Al or Si at two distinct distances, 2.67-2.72 Å and 3.38-3.43 Å These results indicate that the Co bound to the kaolinite surface is octahedrally coordinated, confirming indirect evidence from solution studies that a fraction of sorbed Co forms strongly bound complexes on kaolinite.

Suraj, et al. (1998) studied the adsorption of cadmium and copper by modified kaolinites from Thonnakkal, south Kerala (TK) and Madai, morth Kerala (MK). Amorphous kaolinites were prepared by thermal modification followed by acid activation, which improved their exchangeability. The crystalline structure of kaolinite was thermally transformed to amorphous metakaolin, which on acid activation released preferentially the octahedral aluminium ions from the clay lattice, without disturbing its structure and revealing these sites for substitution with other metal ions. Additional –Al-OH and Si-OH bonds were formed and could also act as cation exchange centers. Adsorption of Cd and Cu on these modified kaolinites was studied as a function of equilibration time and temperature. The exchangeability decreased with increasing calcination temperature (to 600°C) (from 6.34 to 3.08 (Cd) and 6.0 to 3.06 (Cu) mmol/kg for TK and 6.55 to 3.15 (Cd) and 6.21 to 4.16 (Cu) mmol/kg for MK). Uptake of Cd and Cu at 30, 40, 50 and 60°C displayed similar kinetics with maximum uptake at 40°C for both Cd and Cu.

Sarkar, et al. (2000) studied the adsorption of Hg(II) by kaolinite as a function of solution pH, ionic strength, and the competitive or complexation effect of ligands (Cl, SO_4, PO_4) and metals (Ni and Pb). The study showed that Hg(II) adsorption from a 0.6 μM Hg(II) solution was primarily influenced by pH. The Hg(II) adsorption edge was described of 3.4 and a pH_{max} of 4.4. At pH values above the pH_{max}, Hg (II) retention

decreased with increasing pH. Cl and Ni shifted pH_{50} from 3.4 to 7 and 4.1, respectively. Ni and Pb reduced the amount of Hg(II) adsorbed throughout the pH range examined. Ionic strength and the presence of SO_4 and PO_4 had relatively little impact on the Hg(II) adsorption envelope. The results also suggested that Hg(II) adsorption by both – SiOH and –AlOH sites on kaolinite should be considered in order to predict accurately the Hg(II) retention.

Angove, et al. (2001) studied the uptake of anthracene from dilute aqueous solutions onto goethite and kaolinite at 25°C, first in the absence and then in the presence of three benzene carboxylic acids: phthalic acid, trimesic acid, and mellitic acid. Carboxylic acid concentrations were 0.20, 0.10, and 0.05 mM. Anthracence (0.20 μM) did not adsorb strongly onto the pure mineral surface, but in the presence of phthalic acid a substantial increase in anthracene uptake was observed. Anthracene molecules were assumed to interact with adsorbed phthalate. It was proposed that the enhancement of anthracene adsorption in the presence of phthalic acid is due to an increase in the hydrophobicity of the mineral surface once phthalic acid molecules adsorb.

Hong, et al. (2003) studied the adsorption of the $AuCl_4^-$ complex by kaolinites of different crystallinities (Kao-1 and Kao-2) from solutions containing 10,000, 500 and 50 μg/L Au and 1 g of kaolinite at pH 3 - 9 at ambient temperature and 120°C. The study showed that adsorption from the 50, 500, and 10,000 μg Au/L solutions ranged from 64 to 100% at ambient temperature and from 68 to 100% at 120°C for both kaolinites. Adsorption was pH dependent with a maximum at pH < 5 and a minimum at neutral and alkaline pH values. Up to 1 mg Au/g kaolinite was adsorbed by the kaolinites at both ambient temperature and 120°C. In a separate Au adsorption experiment using 100 ml of 4000 μg/L solutions and 0.02 to 1.0 g of Kao-1, up to 8.55 mg Au/g of kaolinite was adsorbed. The pH dependence of Au adsorption suggests that surface complexation of Au to alumina sites at the edges of kaolinite particles might be involved. Protonation of kaolinite surface sites might facilitate adsorption of the anionic Au complex.

Bhattacharry and Gupta (2007) studied the adsorption of Co(II) from aqueous medium on natural and acid activated kaolinite and montmorillonite. Adsorption increased continuously from pH 1.0 to 8.0 after which adsorption could not be carried out due to

the decreasing solubility of Co(II). Under appropriate conditions, the adsorption of Co(II) is very fast, approaching equilibrium within 240 min at low coverage, and the interactions are best described by 2^{nd} order kinetics. It was also found that acid activation enhanced the adsorption capacity of kaolinite and montmorillonite.

Bhattacharry and Gupta (2008) studied the removal of Ni(II) and Cu(II) from aqueous medium by kaolinite, montmorillonite and their acid-activated forms. Batch adsorption experiments were carried out by considering various solution pH values, interaction times, and temperatures. It was found that adsorption was strongly dependent on the pH of the medium. Uptake was very fast initially and maximum adsorption was observed within 180 and 360 min of agitation for Ni(II) and Cu(II), respectively. The kinetics of the interactions were best described by as 2^{nd} order. The adsorption data yielded a Langmuir monolayer capacity of 4.3-28.0 and 7.1-21.3 mg/g for clay-Ni(II) and clay-Cu(II) interaction, respectively. The results showed that kaolinite and montmorillonite and their acid-activated forms are good adsorbents for Ni(II) and Cu(II) in aqueous medium.